HHS Public Access

Author manuscript

Cell Rep. Author manuscript; available in PMC 2019 September 16.

Published in final edited form as:

Cell Rep. 2019 September 03; 28(10): 2647–2658.e5. doi:10.1016/j.celrep.2019.07.105.

Expression of the Mxra8 Receptor Promotes Alphavirus Infection and Pathogenesis in Mice and Drosophila

Rong Zhang[1,5], **James T. Earnest**[1], **Arthur S. Kim**[1,2,3], **Emma S. Winkler**[1,3], **Pritesh Desai**[1], **Lucas J. Adams**[1], **Gaowei Hu**[1,5], **Christopher Bullock**[1,3], **Beth Gold**[6], **Sara Cherry**[6], **Michael S. Diamond**[1,2,3,4,7,*]

[1]Department of Medicine, Washington University School of Medicine, St. Louis, MO 63110, USA

[2]Department of Molecular Microbiology, Washington University School of Medicine, St. Louis, MO 63110, USA

[3]Department of Pathology and Immunology, Washington University School of Medicine, St. Louis, MO 63110, USA

[4]The Andrew M. and Jane M. Bursky Center for Human Immunology and Immunotherapy Programs, Washington University School of Medicine, St. Louis, MO 63110, USA

[5]Key Laboratory of Medical Molecular Virology (MOE/NHC/CAMS), School of Basic Medical Sciences, Shanghai Medical College, Fudan University, Shanghai 200032, China

[6]Department of Microbiology, University of Pennsylvania, Philadelphia, PA 19104, USA

[7]Lead Contact

SUMMARY

Mxra8 is a recently described receptor for multiple alphaviruses, including Chikungunya (CHIKV), Mayaro (MAYV), Ross River (RRV), and O'nyong nyong (ONNV) viruses. To determine its role in pathogenesis, we generated mice with mutant Mxra8 alleles: an 8-nucleotide deletion that produces a truncated, soluble form ($Mxra8^{\Delta 8/\Delta 8}$) and a 97-nucleotide deletion that abolishes Mxra8 expression ($Mxra8^{\Delta 97/\Delta 97}$). $Mxra8^{\Delta 8/\Delta 8}$ and $Mxra8^{\Delta 97/\Delta 97}$ fibroblasts show reduced CHIKV infection in culture, and $Mxra8^{\Delta 8/\Delta 8}$ and $Mxra8^{\Delta 97/\Delta 97}$ mice have decreased infection of musculoskeletal tissues with CHIKV, MAYV, RRV, or ONNV. Less foot swelling is observed in CHIKV-infected Mxra8 mutant mice, which correlated with fewer infiltrating neutrophils and cytokines. A recombinant E2-D71A CHIKV with diminished binding to Mxra8 is attenuated *in vivo* in wild-type mice. Ectopic Mxra8 expression is sufficient to enhance CHIKV

*Correspondence: diamond@wusm.wustl.edu.

AUTHOR CONTRIBUTIONS

R.Z., J.T.E., E.S.W., P.D., S.C., and M.S.D. designed the experiments. R.Z., J.T.E., E.S.W., P.D., L.J.A., and G.H. performed the *in vivo* and mammalian cell culture experiments. A.S.K. performed the structural analysis and the Mxra8 binding assays. B.G. performed the experiments with transgenic flies. R.Z. and M.S.D. wrote the initial draft of the manuscript, with the other authors providing comments and edits to the final version.

SUPPLEMENTAL INFORMATION

Supplemental Information can be found online at https://doi.org/10.1016/j.celrep.2019.07.105.

DECLARATION OF INTERESTS

M.S.D. is a consultant for Inbios and Atreca and serves on the Scientific Advisory Board of Moderna.

infection and lethality in transgenic flies. These studies establish a role for Mxra8 in the pathogenesis of multiple alphaviruses and suggest that targeting this protein may mitigate diseasein humans.

Graphical Abstract

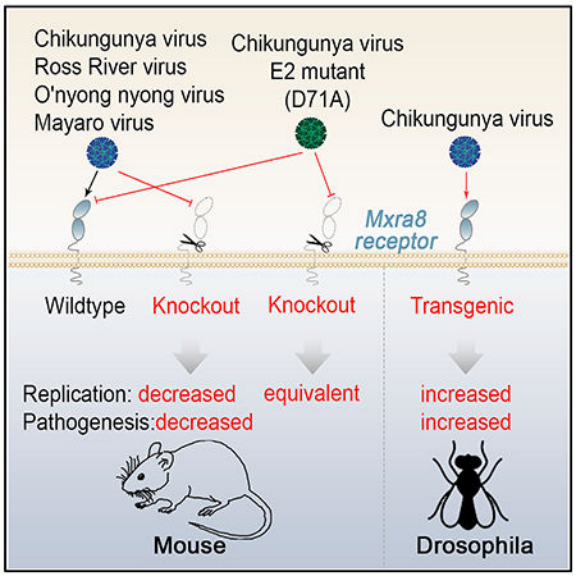

In Brief

Zhang et al. use CRISPR-Cas9 gene editing to generate mice with out-of-frame 8- and 97-nucleotide deletions in Mxra8. These mice show markedly reduced infection of CHIKV, MAYV, RRV, and ONNV during the acute phase. These experiments establish a key role for Mxra8 in the pathogenesis of multiple alphaviruses.

INTRODUCTION

Alphaviruses are single-stranded, positive-polarity enveloped RNA viruses that are among the most important arthropod-transmitted viruses causing disease in humans and other animals (Powers et al., 2001). Alphaviruses are classified into two groups, Old World and New World, based on their genetic relatedness and historical boundaries. Old World alphaviruses include Chikungunya (CHIKV), Mayaro (MAYV), O'nyong'nyong (ONNV), Ross River (RRV), Sindbis (SINV), and Semliki Forest (SFV) viruses, several of which cause epidemic debilitating acute and chronic polyarthritis affecting millions of people globally. New World viruses, which include Eastern (EEEV), Venezuelan (VEEV), and Western (WEEV) equine encephalitis viruses, propagate through enzootic and epizootic cycles and can infect neuronal cells in the brain, resulting in encephalitis and death. With recent global spread, some Old World alphaviruses (e.g., CHIKV) now circulate in both hemispheres. Despite their epidemic potential, there are no licensed therapies or vaccines for any alphavirus infection.

The alphavirus genomes encode four non-structural and five structural proteins using two open reading frames and have a 5′ cap and a 3′ poly(A) tail (Strauss et al., 1994). The non-structural proteins are synthesized from the 49S genomic RNA and are required for virus translation, replication, and immune evasion; the structural proteins (capsid [C] and envelope [E3-E2-6K-E1]) are synthesized from a 26S subgenomic RNA (Cancedda et al., 1975). Among the structural proteins, the E1 envelope glycoprotein contains a hydrophobic peptide that participates in pH-dependent endosomal fusion (Lescar et al., 2001). The E2 envelope glycoprotein binds to attachment and entry factors (Smith et al., 1995; Zhang et al., 2005), which facilitates clathrin-dependent endocytosis (DeTulleo and Kirchhausen, 1998; Lee et al., 2013). The E3 protein is necessary for the folding of p62 (precursor to E2) and the formation of the E2-E1 heterodimer (Carleton et al., 1997; Mulvey and Brown, 1995) but is cleaved during the maturation process in the *trans*-Golgi network (Heidner et al., 1996). Mature alphaviruses form at the plasma membrane and contain a single copy of genomic RNA and a lipid bilayer with 240 embedded E2-E1 heterodimers assembled into 80 trimeric spikes that have T = 4 icosahedral symmetry (Cheng et al., 1995; Kostyuchenko et al., 2011; Paredes et al., 1993; Voss et al., 2010).

Despite studying alphaviruses for >50 years, the basis for their cellular and tissue tropism is not fully understood. Attachment factors such as laminin receptor and heparan sulfate have been shown to enhance viral infection for certain alphaviruses (Gardner et al., 2011; Klimstra et al., 1998; Wang et al., 1992). Natural resistance-associated macrophage protein (NRAMP2) has been described as a cellular receptor for SINV but not for CHIKV or RRV (Rose et al., 2011). The protein prohibitin has been suggested as a CHIKV receptor (Wintachai et al., 2012) but corroborating studies are lacking. In addition, the cell surface proteins T cell immunoglobulin (Ig) and mucin-domain containing protein 1 (TIM-1) and TAM family member AXL, which engage phosphatidylserine ligands, may promote CHIKV infection (Jemielity et al., 2013). We recently used a genome-wide CRISPR-Cas9-based screen in mouse cells to identify the two Ig-like domain containing plasma membrane molecule Mxra8 (also called DICAM, Asp3, and Limitrin) as a cellular entry receptor for multiple arthritogenic alphaviruses, including CHIKV, RRV, MAYV, and ONNV (Zhang et al., 2018). The human ortholog MXRA8 also bound to CHIKV and other alphaviruses and facilitated the infection of human fibroblasts, skeletal muscle cells, and chondrocytes. Mxra8 bound directly to CHIKV particles and enhanced attachment and internalization into cells, and Mxra8-Fc fusion protein or anti-Mxra8 monoclonal antibodies (mAbs) blocked CHIKV infection of both mouse and human cells.

Here, to examine the role of Mxra8 in alphavirus pathogenesis, we used CRISPR-Cas9 gene editing to generate mice with out-of-frame 8 (Δ8) and 97 (Δ97) nucleotide (nt) deletions in Mxra8. These mice were born in normal Mendelian frequencies and showed no defects in development, growth, or fecundity. The Δ8 and Δ97 deletions in Mxra8 produced a truncated, soluble form of the ectodomain or no intact protein, respectively. In cell culture, murine embryonic fibroblasts (MEFs) from the $Mxra8^{\Delta 8/\Delta 8}$ and $Mxra8^{\Delta 97/\Delta 97}$ mice had markedly reduced infection by CHIKV compared to wild-type (WT) MEFs. The inoculation of $Mxra8^{\Delta 8/\Delta 8}$ or $Mxra8^{\Delta 97/\Delta 97}$ mice with CHIKV, MAYV, RRV, or ONNV resulted in markedly diminished, yet not abolished, infection of musculoskeletal tissues. Thus, cell surface expression of Mxar8 is required for optimal infection by multiple alphaviruses *in*

vivo, although alternative cell entry pathways exist. In the context of CHIKV infection, mutation and loss of function of Mxra8 were associated with reduced neutrophil infiltration, decreased inflammation, diminished joint swelling, and lower levels of viral RNA at 28 days post-infection (dpi). Reciprocally, a recombinant mutant CHIKV (D71A), which shows loss of binding to Mxra8, specifically showed reduced infection in WT mice compared to the parental virus, although the two replicated equally, albeit at lower levels, in *Mxra8*$^{\Delta 8/\Delta 8}$ mice. Moreover, in *Drosophila*, which lack endogenous expression of Mxra8 or any apparent ortholog, ectopic expression of Mxra8 transgenes resulted in increased CHIKV infection and lethality. Overall, these experiments establish that the entry receptor Mxra8 is required for optimal *in vivo* infection, dissemination, and pathogenesis of multiple alphaviruses.

RESULTS

Generation of Mxra8-Deficient Mice

Since the mouse *Mxra8* gene locus has two full-length transcripts and a short putative transcript near its 3′ end (Figure 1A), we designed two single guide RNAs (sgRNAs) to target a conserved region in all isoforms for CRISPR-Cas9 gene editing (Figures 1A and 1B). After screening the guide sequences for minimal off-target effects, each sgRNA was complexed with the WT Cas9 protein and introduced into day 0.5 C57BL/6J embryos (embryonic day [E] 0.5) via electroporation; two out-of-frame deletion variants (Δ8 and Δ97 nt) were identified by sequencing DNA isolated from pups (Figures 1B and S1A). These mice were backcrossed twice to establish germline transmission and bred to either heterozygosity (*Mxra8*$^{+/\Delta 8}$) or homozygosity (*Mxra8*$^{\Delta 8/\Delta 8}$ and *Mxra8*$^{\Delta 97/\Delta 97}$) for experimentation. Both *Mxra8*$^{\Delta 8/\Delta 8}$ and *Mxra8*$^{\Delta 97/\Delta 97}$ lines showed normal development, growth characteristics, and fecundity.

The Δ8 and/or Δ97 deletion variants could express truncated, soluble forms of Mxra8 due to our targeting of a downstream common exon within the Ig-like domain 2 of Mxra8 (Figure 1B). Regardless, we hypothesized that they may mitigate alphavirus replication because cell surface receptor-dependent internalization is required for infection (Hoornweg et al., 2016). To evaluate this possibility, we generated primary MEFs from WT, *Mxra8*$^{\Delta 8/\Delta 8}$, and *Mxra8*$^{\Delta 97/\Delta 97}$ mice and performed western blotting on the cell lysates and supernatants with two anti-Mxra8 mAbs (Zhang et al., 2018). In the cell lysate, a ~52-kDa Mxra8 band was apparent in WT cells, and a ~34-kDa band was present in *Mxra8*$^{\Delta 8/\Delta 8}$ cells; no specific band was detected in *Mxra8*$^{-\Delta 97/\Delta 97}$ cell lysate (Figure 1C). A ~34-kDa band also was detected in the *Mxra8*$^{\Delta 8/\Delta 8}$ MEF supernatant but not in that from WT or *Mxra8*$^{\Delta 97/\Delta 97}$ cells (Figure 1D). The western blotting results were consistent with the deletion sites: the Δ8 deletion causes a truncation of 12 amino acids C-terminal to the last β strand of domain 2, whereas the Δ97 deletion results in a truncation of the G-strand in domain 2, which is predicted to compromise the integrity of the Ig-like fold (Basore et al., 2019; Song et al., 2019) (Figure 1B). Surface expression of Mxra8 was absent in both *Mxra8*$^{\Delta 8/\Delta 8}$ and *Mxra8*$^{\Delta 97/\Delta 97}$ cells, as determined by flow cytometry (Figure S1B). To assess whether the deletions in Mxra8 affected CHIKV infectivity in cell culture, we performed multi-step growth analysis with WT, *Mxra8*$^{\Delta 8/\Delta 8}$, and *Mxra8*$^{\Delta 97/\Delta 97}$ primary MEFs. CHIKV infection was reduced in both *Mxra8*$^{\Delta 8/\Delta 8}$ and *Mxra8*$^{\Delta 97/\Delta 97}$ MEFs compared to WT cells (Figure 1E), confirming the

loss-of-function phenotype in cells expressing a truncated, soluble variant or no Mxra8 protein at all.

We next examined which cell types and tissues expressed Mxra8 in WT mice. A prior study generated a rabbit polyclonal serum against the 192 N-terminal amino acids of DICAM (an alias of Mxra8) for immunohistochemistry and reported Mxra8 expression on epithelial, myeloid, and mesenchymal cells (Jung et al., 2008). Despite numerous attempts, we were unable to reproduce these findings on either fixed or frozen tissue sections with anti-Mxra8 mAbs, affinity-purified rabbit polyclonal IgG against the Mxra8 ectodomain, or polyclonal rabbit serum elicited against the same 192 N-terminal amino acids of Mxra8. In lieu of these results, we performed RNA *in situ* hybridization (ISH) in musculoskeletal-associated tissues, a relevant site of arthritogenic alphavirus infection, with Mxra8-specific and -negative control probes. Mxra8 mRNA was detected in skin fibroblasts, bone marrow, and synovium (Figure S2A), which is consistent with expression patterns observed from mouse RNA Atlas data (https://oncoscape.v3.sttrcancer.org/atlas.gs.washington.edu.mouse.rna/genes). We also measured Mxra8 mRNA levels in tissues of uninfected and CHIKV-infected mice using qRT-PCR (Figures S2B and S2C). Roughly equivalent expression was detected in musculoskeletal tissues and visceral organs, with slightly lower levels measured in lymph nodes.

Impact of Mxra8 on Acute CHIKV Infection *In Vivo*

To begin to define the contribution of Mxra8 in alphavirus pathogenesis, we inoculated CHIKV (Asian strain AF15561) subcutaneously in the feet of WT and Mxra8 mutant mice. To monitor viral spread at the earliest stages of infection, we measured CHIKV titers in the ipsilateral (to the site of virus injection) ankle at 12 h post-infection (hpi) and viremia at 1 and 2 dpi. Reduced levels of CHIKV infection were observed 12 hpi in the ipsilateral ankle of $Mxra8^{\Delta 8/\Delta 8}$ compared to WT mice (5-fold, $p < 0.01$) (Figure 2A). Consistent with these data, lower levels of CHIKV RNA were detected in the serum of $Mxra8^{\Delta 8/\Delta 8}$ mice at 1 and 2 dpi (5- to 16-fold, $p < 0.05$) (Figure 2B). Next, we measured the amount of infectious virus and foot swelling in WT, $Mxra8^{+/\Delta 8}$, $Mxra8^{\Delta 8/\Delta 8}$, and $Mxra8^{\Delta 97/\Delta 97}$ mice at 3 dpi, a time point that corresponds to the first peak of clinical disease in mice (Morrison et al., 2011). Notably, ipsilateral foot swelling at 3 dpi was nearly abrogated in both $Mxra8^{\Delta 8/\Delta 8}$ and $Mxra8^{\Delta 97/\Delta 97}$ mice and reduced in heterozygous $Mxra8^{+/\Delta 8}$ compared to the WT mice (Figures 2C and 2G). Smaller differences (2- to 4-fold, $p < 0.05$) in viral titers were observed in the ipsilateral ankle of $Mxra8^{\Delta 8/\Delta 8}$ and $Mxra8^{\Delta 97/\Delta 97}$ mice at 3 dpi compared to WT mice, and no difference was observed in the $Mxra8^{+/\Delta 8}$ mice (Figures 2D and 2H). However, larger reductions in viral burden were observed in the ipsilateral calf muscle (11-to 45-fold, $p < 0.001$), contralateral ankle (30- to 50-fold, $p < 0.001$), and contralateral calf muscle (5- to 15-fold, $p < 0.01$) in $Mxra8^{\Delta 8/\Delta 8}$ and $Mxra8^{\Delta 97/\Delta 97}$ mice compared to WT mice (Figures 2D, 2E, 2H, and 2I). We observed a trend toward a reduction in virus titers in the calf muscles of $Mxra8^{+/\Delta 8}$ mice at 3 dpi. We expanded the time course and examined viral infection at 7 dpi, which represents the second peak of clinical disease in mice. Decreases in CHIKV titers were observed in the ipsilateral ankle of $Mxra8^{\Delta 8/\Delta 8}$ compared to WT mice at 7 dpi (18-fold, $p < 0.01$) (Figure 2F). To define the role of Mxra8 in CHIKV tropism, we performed RNA ISH on the ipsilateral and contralateral ankles at 3 dpi.

Relatively minor differences were observed with viral RNA ISH in the ipsilateral ankle (Figure 2M), which is consistent with the small reduction in viral titers (Figures 2D and 2H). However, in the contralateral ankle, CHIKV RNA was detected readily in the dermis, synovium, and muscle cells of WT but not *Mxra8*$^{\Delta 8/\Delta 8}$ mice (Figure 2M).

We also infected WT and *Mxra8*$^{\Delta 8/\Delta 8}$ mice with CHIKV LR 2006, an East/Central/South African strain that showed less dependence on the Mxra8 entry pathway in cell culture (Zhang et al., 2018). Nonetheless, we observed similar *in vivo* results with CHIKV LR 2006 and AF15561 strains. Decreased swelling and reduced virus titers in the ipsilateral and contralateral ankles and calf muscles were observed in CHIKV LR 2006-infected *Mxra8*$^{\Delta 8/\Delta 8}$ mice, and spread to tissues distal from the site of inoculation was greatly diminished (Figures 2J–2L). To evaluate whether the soluble, truncated Mxra8 protein generated from the 8-nt frameshift deletion had any effect on CHIKV infection, *Mxra8*$^{\Delta 8/\Delta 8}$ mice were administered PBS, an isotype control mAb, or two anti-Mxra8 blocking mAbs (1G11.E6 + 7F1.D8) (Zhang et al., 2018) 12 h pre-CHIKV inoculation. At 3 dpi, no differences in viral load were detected in the ipsilateral and contralateral ankles and calf muscles of *Mxra8*$^{\Delta 8/\Delta 8}$ mice treated with PBS or the control or anti-Mxra8 mAbs (Figure S3); these data suggest that soluble Mxra8 did not independently affect CHIKV infection. Overall, these experiments establish the following: (1) *Mxra8*$^{\Delta 8/\Delta 8}$ (truncated, soluble protein) and *Mxra8*$^{\Delta 97/\Delta 97}$ (protein null) mice phenocopy each other in the context of CHIKV infection and joint swelling, (2) small differences in CHIKV infection are observed with Mxra8 haploinsufficiency, (3) the absence of Mxra8 modulates virus spread to a greater extent than replication at the local site of injection, (4) two CHIKV strains with varying Mxra8 dependency in cell culture showed similar clinical and virological phenotypes in Mxra8 mutant mice.

Our subcutaneous inoculation model suggests that Mxra8 has a greater role in CHIKV dissemination than local infection. We speculated this could reflect a cell type-specific Mxra8-independent entry pathway in the tissues of the foot or unique growth kinetics of CHIKV in the absence of early innate immune responses. To begin to address this question, we inoculated intravenously WT and *Mxra8*$^{\Delta 8/\Delta 8}$ mice with CHIKV-AF15561 and monitored infection at 1 and 3 dpi. Notably, reduced virus titers were observed in both the ankles and calf muscles of *Mxra8*$^{\Delta 8/\Delta 8}$ compared to WT mice (Figures 3A and 3B). The disparity in infection of ipsilateral and contralateral ankles in WT and Mxra8 mutant mice after subcutaneous and intravenous inoculation suggests that additional factors (e.g., local innate immunity) may modulate the kinetics of CHIKV growth.

Impact of Mxra8 on Other Arthritogenic Alphavirus Infections *In Vivo*

We next evaluated MAYV, RRV, and ONNV infection in Mxra8 mutant mice. Similar to results observed with CHIKV, reductions in MAYV-induced foot swelling were observed in *Mxra8*$^{\Delta 8/\Delta 8}$ compared to WT mice at 3 dpi (Figure 4A). We also observed a phenotype with MAYV spread, as there was a significant decrease in virus titers in the ipsilateral calf muscle (14-fold, $p < 0.0001$), draining lymph node (9-fold, $p < 0.01$), contralateral ankle (10-fold, $p < 0.05$), and contralateral calf muscle (4-fold, $p < 0.01$), but not in the ipsilateral ankle (4-fold, $p > 0.05$) at 3 dpi (Figures 4B–4D). In an RRV infection model, which does not cause

joint swelling (Morrison et al., 2006), we observed reduced virus titers in the ipsilateral ankle (15-fold, $p < 0.0001$), ipsilateral calf muscle (6-fold, $p < 0.01$), contralateral ankle (11-fold, $p < 0.0001$), and contralateral calf muscle (4-fold, $p < 0.01$) of *Mxra8*$^{\Delta 8/\Delta 8}$ mice at 3 dpi (Figures 4E and 4F). In an ONNV infection model, virus titers in the ipsilateral ankle were reduced (7-fold, $p < 0.01$) in *Mxra8*$^{\Delta 8/\Delta 8}$ compared to WT mice at 1 dpi (Figure 4G); later time points and other tissues were not analyzed, as ONNV infection is rapidly controlled by interferon (IFN) responses in immunocompetent mice (Fox et al., 2015; Seymour et al., 2013).

Impact of Mxra8 on Subacute Alphavirus Infection and Persistence

Subcutaneous CHIKV infection in mice results in prolonged foot swelling lasting 2-3 weeks and persistent viral RNA in joint-associated tissues for months, which is associated with the histopathological evidence of synovitis, arthritis, and tendonitis (Hawman et al., 2013). We tested the impact of Mxra8 on ankle swelling during the first month of infection. Compared to WT animals, *Mxra8*$^{\Delta 8/\Delta 8}$ mice inoculated with CHIKV-AF15561 showed markedly reduced foot swelling during the first two peaks of swelling at 2–3 dpi and 6–8 dpi, respectively (Figure 5A). At 28 dpi, lower levels (12-fold, $p < 0.0001$) of CHIKV RNA were detected in the ipsilateral ankle of *Mxra8*$^{\Delta 8/\Delta 8}$ mice (Figure 5B). To corroborate these results, anti-Mxra8-blocking mAbs (Zhang et al., 2018) were administered via an intraperitoneal route to WT mice at 12 h pre- (Figure 5C) or post- (Figure 5D) infection and subsequently every 4 days. Similar to results with *Mxra8*$^{\Delta 8/\Delta 8}$ mice, reduced foot swelling was also observed with either prophylactic or therapeutic administration of anti-Mxra8 mAbs.

CHIKV-Induced Inflammation in *Mxra8*$^{\Delta 8/\Delta 8}$ Mice

Given the reduction in swelling of the ipsilateral ankles of *Mxra8*$^{\Delta 8/\Delta 8}$ mice, we analyzed the impact of Mxra8 on immune cell accumulation at 3 and 7 dpi, which corresponds to the infiltration of myeloid cells (monocytes and neutrophils) and pathogenic $CD4^+$ T cells (Haist et al., 2017; Poo et al., 2014; Teo et al., 2013), respectively, in mice (Figure 6). In uninfected mice (day 0), as expected, relatively few $CD45^+$ leukocytes were present in the joint homogenates; however, we did observe small reductions in some cell types (e.g., neutrophils, macrophages, dendritic cells) at baseline in *Mxra8*$^{\Delta 8/\Delta 8}$ mice compared to WT mice (Figure 6B). At 3 dpi, despite the large differences in tissue swelling and edema (Figure 6A), the numbers of most immune cell populations had increased and were similar between WT and *Mxra8*-mutant mice (Figures 6C and S4); however, differences were observed in the number of neutrophils (2-fold decrease, $p < 0.05$) and dendritic cells (3-fold increase, $p < 0.001$) in *Mxra8*$^{\Delta 8/\Delta 8}$ mice. At 7 dpi, similar results were observe with a decrease in neutrophils (5-fold, $p < 0.0001$) and an increase in dendritic cells (2-fold, $p < 0.05$) in *Mxra8*$^{\Delta 8/\Delta 8}$ mice (Figure 6D).

To gain further insight into the effect of Mxra8 on CHIKV-induced joint inflammation, we profiled cytokines and chemokines in ipsilateral ankles at 3 and 7 dpi in WT and *Mxra8*$^{\Delta 8/\Delta 8}$ mice. Although many were undetectable (e.g., interleukin-2 [IL-2], IL-3, IL-4, IL-5, IL-13, and IL-17), several pro-inflammatory cytokines and chemokines were reduced in the joint homogenates of *Mxra8*$^{\Delta 8/\Delta 8}$ mice, including IL-1β (7 dpi), IL-6 (3 dpi), IL-12 (p40) (7 dpi),

IFN-γ (7 dpi), tumor necrosis factor α (TNF-α) (7 dpi), granulocyte colony-stimulating factor (G-CSF) (3 and 7 dpi), granulocyte-macrophage CSF (GM-CSF) (3 and 7 dpi), monocyte chemoattractant protein 1 (MCP-1) (7 dpi), macrophage inflammatory protein 1α (MIP-1α) (7 dpi), MIP-1β (3 and 7 dpi), RANTES (7 dpi), and CXCL1 (7 dpi) (Figures 6E and S5). Thus, even the moderate reductions in CHIKV virus titers in the ipsilateral foot at 3 and 7 dpi were associated with marked decreases in levels of multiple pro-inflammatory mediators, which likely affected the clinical swelling phenotype.

A Mutant CHIKV with Diminished Mxra8 Binding Is Attenuated Specifically in WT Mice

Two groups recently showed that Mxra8 binds to CHIKV by wedging into a cleft created by two adjacent E2-E1 heterodimers within a trimeric spike (Basore et al., 2019; Song et al., 2019). Several solvent-exposed residues in the A domain of E2 (e.g., D71) were predicted to form key contacts with Mxra8 directly (Figure 7A), and E2-6K-E1 expression constructs with these mutations decreased Mxra8 binding in transfection experiments in cells (Zhang et al., 2018). As an independent method of determining the contribution of Mxra8 to CHIKV pathogenesis, we generated the D71A mutation in CHIKV (AF15561 strain background). We confirmed that the mutant D71A CHIKV had a diminished ability to bind Mxra8 in a modified virus capture ELISA (Figure 7B). Subsequently, we inoculated WT and D71A CHIKV into WT and $Mxra8^{\Delta 8/\Delta 8}$ mice. At 3 dpi, compared to the parental WT virus, D71A CHIKV showed reduced infection in the ipsilateral and contralateral ankles (5- to 14-fold, $p < 0.01$) and the ipsilateral and contralateral (12- to 13-fold, $p < 0.05$) calf muscles in WT mice (Figure 7C). However, no difference in infection between the WT and D71A CHIKV was detected in the ankles of $Mxra8^{\Delta 8/\Delta 8}$ mice, although the levels of parental virus were lower than in WT mice. Thus, a loss-of-Mxra8-binding mutant CHIKV is attenuated compared to the WT virus only in animals expressing intact forms of Mxra8.

Ectopic Expression of Mxra8 in *Drosophila* Enhances CHIKV Pathogenicity

A BLAST alignment of Mxra8 revealed orthologs in mammals, birds, reptiles, and fish but none in invertebrate animals (Zhang et al 2018) even though the transmission of arthritogenic alphaviruses requires an amplification stage in mosquito hosts. Although our experiments in mice establish that Mxra8 expression is necessary for optimal infection and pathogenesis, we set out to determine whether it would be sufficient to enhance infection *in vivo.* To test this, we created transgenic flies that ectopically express mouse Mxra8 (Figure 7D). Uninfected flies expressing Mxra8 showed no difference in survival rates compared to transgenic control flies. As in mosquitoes, infection of WT flies with arboviruses such as CHIKV (strain 181/25) have no impact on mortality (Figure 7E). In comparison, Mxra8-expressing flies infected with CHIKV showed greater mortality rates, and this phenotype was associated with higher levels in viral RNA in whole flies (Figures 7E and 7F). Thus, ectopic expression of Mxra8 in flies is sufficient to enhance infection and disease in invertebrate animals that do not normally succumb to infection and lack this alphavirus receptor.

DISCUSSION

In a prior study, we defined the cell surface protein Mxra8 as an entry receptor for CHIKV and other related arthritogenic alphaviruses (Zhang et al., 2018). Here, we assessed the role of Mxra8 in alphavirus infection using genetically engineered Mxra8 mutant mice to study tissue tropism, viral pathogenesis, and the ensuing immune response. Introduction of either 8- or 97-nt frameshift deletions in domain 2 of mouse Mxra8, which generated a soluble protein or no protein at all, resulted in markedly reduced foot swelling and dissemination of CHIKV. Haploinsufficiency was observed, as less swelling and reduced viral burden occurred in CHIKV-infected *Mxra8*$^{+/\Delta 8}$ mice. Associated with the reductions in CHIKV infection were diminished accumulation of neutrophils and lower levels of pro-inflammatory cytokines in musculoskeletal-associated tissues. Loss of cell surface Mxra8 expression also mitigated CHIKV persistence and resulted in the reduced infection of MAYV, RRV, and ONNV, three additional emerging arthritogenic alphaviruses. Compared to a parental WT virus, a recombinant CHIKV (D71A) encoding a loss-of-Mxra8-binding substitution was attenuated specifically in WT but not *Mxra8*$^{\Delta 8/\Delta 8}$ mice. Moreover, ectopic expression of Mxra8 in transgenic *Drosophila* was sufficient to increase CHIKV replication and mortality. Overall, these experiments establish a key role for Mxra8 in the infection, dissemination, and pathogenesis of multiple related arthritogenic alphaviruses *in vivo.*

The physiological function of Mxra8 is not fully understood. Mxra8 was first called adipocyte-specific protein 3 (ASP3), as it is upregulated during adipocyte differentiation and expressed in mesenchymally derived cells (Jung et al., 2004). High levels of mRNA expression of its bovine ortholog were observed in skeletal muscle tissue with high marbling and fat content (Clark et al., 2011). Mxra8 was also called limitrin, because of its expression in the glia limitans and speculated function in maintaining the blood-brain barrier (Yonezawa et al., 2003). Given its predicted Ig-like domains and cell surface expression pattern, Mxra8 was called DICAM (Jung et al., 2008) and shown *in vitro* to bind to the αVβ3 integrin, resulting in attenuated αVβ3 signaling and suppression of osteoclast differentiation and angiogenesis (Han et al., 2013; Jung et al., 2008, 2012). Mxra8 also has been shown to promote the proliferation and maturation of chondrocytes (Han et al., 2018). More recently, in a study with independently generated Mxra8-deficient mice, Mxra8 (DICAM) exhibited a protective role in experimental colitis by stabilizing the integrity of junctional complexes in the intestinal mucosal barrier (Han et al., 2019). Although our experiments do not directly address the physiological function of Mxra8, the generation of viable and fertile protein null gene-edited mice by us and others (Han et al., 2019) is consistent with a non-essential role in cell survival, development, and homeostasis. The human ortholog of Mxra8 was not identified as an essential gene in several cell types subjected to genome-wide CRISPR editing and survival analysis (Wang et al., 2015). Our *in situ* hybridization analysis identified Mxra8 RNA in fibroblasts and cells in the synovium, which is consistent with the targets and tropism of arthritogenic alphavirus infection in musculoskeletal-associated tissues (Morrison et al., 2006, 2011; Sourisseau et al., 2007). Nonetheless, despite repeated attempts with multiple monoclonal and polyclonal antibodies, we were unable to detect reliably the Mxra8 protein expression pattern in tissues that one group has reported (Jung et al., 2008, 2012). The generation of Mxra8 reporter gene mice

may be required to fully delineate its expression pattern and elucidate its possible functions in connective tissues and other sites.

One prominent phenotype we observed was the nearly abolished joint swelling despite rather modest reductions in CHIKV burden at day 3 in the ipsilateral ankle of Mxra8-deficient mice when the virus was administered in the foot at a proximal site. These results are consistent with our prior study using function-blocking mAbs against Mxra8 (Zhang et al., 2018). At this early time point in CHIKV pathogenesis in mice, the host innate immune response exerts a dominant function in modulating inflammation, and this is mediated in part by vasoactive cytokines and infiltrating monocytes and neutrophils (Fox et al., 2019; Poo et al., 2014). In joint-associated tissues of CHIKV-infected Mxra8-deficient mice, we detected reduced numbers of neutrophils and increased dendritic cells, the latter of which express regulatory receptors that can mitigate CHIKV-induced arthritis and edema (Long et al., 2013); some of this difference in foot swelling after CHIKV infection could have been affected by the slight differences in immune cell numbers in musculoskeletal tissues observed at baseline between WT and Mxra8-deficient mice. Associated with this were reduced tissue homogenate levels of several pro-inflammatory mediators, including IL-6, G-CSF, GM-CSF, and MIP-1β, in Mxra8-deficient compared to WT mice. The basis for the ostensible discrepancy between the marked effect of Mxra8 expression on foot swelling and the smaller effect on CHIKV infection warrants further study. Possible explanations include a non-linear relation between infection and joint inflammation; an independent effect of Mxra8 signaling on inflammation; or local interactions between CHIKV, Mxra8, and the innate immune response in the foot. However, when we inoculated CHIKV via an intravenous route, equivalent reductions in viral burden were observed in both ankles, suggesting that the tropism of the virus in the foot and associated musculoskeletal tissues can vary, depending on the pathogenesis sequence.

Our prior studies in cell culture with CHIKV suggested that while Mxra8 was a dominant receptor for entry and infection, a second, Mxra8-independent pathway must exist because low levels of infection were observed in gene-edited fibroblasts for Mxra8 or in other cell types that endogenously do not express Mxra8 (Zhang et al., 2018). Our infection studies in $Mxra8^{\Delta 8/\Delta 8}$ or $Mxra8^{\Delta 97/\Delta 97}$ mice are consistent with this observation. Although markedly reduced infection was measured in the gene-edited mice, alphavirus replication clearly occurred in the absence of Mxra8 expression. Both strains of CHIKV (Asian AF15561 and East/Central/South African LR 2006) showed equivalent loss-of-infection phenotypes *in vivo*, even though we previously observed a differential Mxra8 dependence in NIH 3T3 cells. The basis for this apparent discrepancy between cell culture and mouse data remains uncertain, although it could be due to differences in the cell type-specific expression of the Mxra8-independent ligand in culture and *in vivo.* The identity of the alternative, Mxra8-independent entry ligand also remains unknown, and the precise function of Mxra8 in attachment, entry, and trafficking of alphavirus virions remains to be established. Possible alternative binding ligands that require future investigation include heparan sulfate proteoglycans (Gardner et al., 2011; Klimstra et al., 1998; Silva et al., 2014), prohibitin (Wintachai et al., 2012), NRAMP2 (Rose et al., 2011), and TIM and TAM family members proteins that bind phosphatidylserine moieties (Jemielity et al., 2013). The ability to cross putative ligand-deficient mice onto a Mxra8-deficient background or treat such animals with

Mxra8 function blocking mAbs may help to elucidate the residual entry pathway of CHIKV and possibly other alphaviruses. Alternatively, genetic screens (small interfering RNA [siRNA], small hairpin RNA [shRNA], or CRISPR-based) can be performed in Mxra8-deficient cells with a loss-of-CHIKV infection readout to define the residual pathway of entry.

The existence of a second entry pathway for CHIKV in mammals is consistent with the observation that lower organisms, such as mosquitoes, which do not encode an Mxra8 ortholog, transmit this virus in nature. The identity of this secondary entry receptor for CHIKV in mammals and its possible relation to the one in insects remains to be defined. Nevertheless, ectopic expression of Mxra8 rendered flies more susceptible to infection with increased replication and mortality. For mosquito transmission, arboviruses must replicate to high enough titers for efficient transfer to vertebrates during a blood meal, but not so high that pathogenesis occurs in the infected mosquito. The loss of innate immune control of arboviruses in insects leads to increased replication and mortality (Liu et al., 2018; Merkling and van Rij, 2013). Our data suggest that higher levels or ectopic expression of receptors in insects also can shift this balance away from controlled levels of arbovirus infection.

In summary, we generated Mxra8 mutant mice by introducing out-of-frame deletions within and adjacent to the second Ig-like domain. Where the 8-nt deletion resulted in a truncated, soluble Mxra8, the 97-nt deletion was a protein null. Both mice showed marked reductions in CHIKV infection and swelling and appeared to phenocopy each other. Similar results were observed in the $Mxra8^{\Delta 8/\Delta 8}$ mice after inoculation with three other arthritogenic alphaviruses, MAYV, RRV, and ONNV. No obvious developmental or growth defects were observed in our two founder lines, which is consistent with an Mxra8-deficient mouse generated by another laboratory studying experimental colitis (Han et al., 2019). Although future studies are required to define fully the endogenous functions of Mxra8, its transient blockade with antibodies or small molecules could represent a plausible therapeutic strategy to prevent or treat infections by multiple globally emerging arthritogenic alphaviruses with epidemic potential.

STAR★METHODS

LEAD CONTACT AND MATERIALS AVAILABILITY

Further information and requests for resources and reagents should be directed to and will be fulfilled by the Lead Contact author Michael S. Diamond (diamond@wusm.wustl.edu). All plasmids, antibodies, cells, viruses, and mouse lines developed for this study are available under Material Transfer Agreements from Washington University.

EXPERIMENTAL MODEL AND SUBJECT DETAILS

Viruses—The following viruses were used in the study: CHIKV (LR 2006, AF15561, and 181/25), RRV (T48), MAYV (BeH407), and ONNV (MP30). All viruses were propagated in Vero cells and titrated by focus-forming assays, as described previously (Zhang et al., 2018). The CHIKV AF15561 D71A mutant was generated by overlapping PCR. The genomic RNA was transcribed *in vitro* from cDNA using the mMESSAGE mMACHINE SP6 Transcription

Kit (ThermoFisher scientific, AM1340), purified, and electroporated into BHK21 cells to rescue the virus. The mutant virus was passaged once in Vero cells and titrated by focus-forming assay (Zhang et al., 2018). The region encompassing the structural genes (C-E3-E2-6K-E1) was confirmed by sequencing before use.

Generation of Mxra8 deficient mice—The sequence of Mxra8 locus (NC_000070.6) was obtained from NCBI, and two sgRNAs targeting the common exon were designed based on the RefSeq annotations, which have two nearly identical transcripts and one short, putative transcript. The two sgRNAs also were selected based on their low off-target profile and absence of single nucleotide polymorphisms: sgRNA-1, 5′-GGAAGACTCGGCGCTCGTGG-3′; sgRNA-2, 5′-CTGTGACCAGACCCATTGCC-3′. The two gRNAs containing the scaffold were generated by *in vitro* synthesis (HiScribe T7 *In Vitro* Transcription Kit, New England BioLabs) followed by cleanup purification (MEGAclear Transcription Clean-Up Kit, Thermo Fisher). Guide RNAs and Cas9 protein were complexed and electroporated into C57BL/6 zygotes simultaneously in C57BL/6J mice. After genotyping and two rounds of backcrossing, founder lines with 8- or 97-nt frameshift deletions within Mxra8 were generated. The homozygous and heterozygous mice were used for experiments. The generation of deleted mice was accomplished with the aid of the Genome Engineering and iPSC center and Department of Pathology Micro-Injection Core (Washington University School of Medicine).

Mouse experiments—Experiments were carried out in accordance with the recommendations in the Guide for the Care and Use of Laboratory Animals of the National Institutes of Health after approval by the Institutional Animal Care and Use Committee at the Washington University School of Medicine (Assurance number A3381-01). Four week-old WT, Mxra8$^{+/\Delta 8}$, Mxra8$^{\Delta 8/\Delta 8}$, and Mxra8$^{\Delta 97/\Delta 97}$ male or female C57BL/6J mice were inoculated subcutaneously in the footpad with 10^3 FFU of CHIKV (AF15561 or LR 2006 strains), MAYV, RRV, or ONNV. At 12 h, day 1, 2, 3, or 7 post-infection, animals were euthanized, and after extensive perfusion with PBS, indicated tissues were collected. Ipsilateral ankle joint swelling (width × height) was monitored using digital calipers as previously described (Hawman et al., 2013). To assess the long-term effect of CHIKV infection, the ipsilateral feet were collected for viral RNA quantification. Similarly, for antibody pre- or post-treatment experiments, 300 mg of purified Armenian hamster mAbs (1G11.E6 + 7F1.D8) or isotype control (Bio X Cell # BE0260) in PBS were administered via an intraperitoneal route to four week-old WT male C57BL/6 mice either 12 h before or after subcutaneous inoculation in the footpad with 10^3 FFU of CHIKV-AF15561. The mice also were administered mAbs at 4 and 8 dpi, and joint swelling was measured for 12 days. For intravenous inoculation experiments, mice were injected via the tail vein with 10^3 FFU of CHIKV AF15561, and tissues were harvested at 1 and 3 dpi for viral burden analysis. Blinding and randomization were not performed.

Fly infections—Mouse *Mxra8* (NM_024263) gene sequences was codon-optimized for *Drosophila*, synthesized with a *Drosophila* Kozak-like sequence (CAAA) and a 3′ FLAG tag, and inserted into a NotI and XhoI digested pUASTattB vector using In-Fusion Cloning. Transgenic flies were generated after integrating the Mxra8 transgene into Chromosome 2

attB (Rainbow Transgenics). Flies were verified, and homozygous males or WT males were crossed to female flies expressing Actin-GAL4 to drive ubiquitous expression of the transgenes. Groups of ~20 adult 7 to 10 day-old male flies (control (Actin > +) or expressing the transgene (Actin > *Mxra8)*) were inoculated with 3×10^3 PFU of CHIKV (strain 181/25). Survival was monitored daily in three independent experiments. Groups of 15 adult 7 to 10 day-old female flies were inoculated with 3×10^3 PFU of CHIKV (181/25) and were subsequently crushed in TRIzol (Thermo Fisher) at 7 dpi. Total RNA was purified, and RT-qPCR was performed using virus-specific primers (5′-Forward: GGCAGTGGTCCCAGATAATTCAAG, 5′-Reverse: ACTGTCTAGATCCACCCCATACATG) and normalized to the housekeeping gene rp49 (5′-Forward: AAGAAGCGCACCAAACACTTCATC, 5′-Reverse: TCTGTTGTCGATACCCTTCGGCTT).

METHOD DETAILS

Viral growth kinetics analysis—Primary MEFs (sex unknown) were generated from E15 to E16 mouse embryos and maintained in DMEM supplemented with 10% FBS, non-essential amino acids, and penicillin and streptomycin. Cells in 12-well plates were inoculated with CHIKV AF15561 at a multiplicity of infection (MOI) of 0.01 for 1 h, washed twice and maintained in culture medium supplemented with 2% FBS. Supernatants were collected at specific times after infection for virus titration on Vero cells by focus-forming assay (Pal et al., 2013).

Mxra8 ELISA binding assay—Maxisorp ELISA plates were coated with 2 μg/ml of anti-CHIKV mAbs CHK-152 and CHK-166 (Pal et al., 2013) overnight in sodium bicarbonate buffer (pH 9.3). Plates were washed four times with 1X PBS and blocked for 1 h at 25°C with 4% BSA. CHIKV AF15561 wild-type and D71A mutant viruses were diluted to 10^6 FFU/ml in 2% BSA and added to plates (50 μl/well) for 1 h at 25°C. Plates were washed five times with PBS and incubated with 10 μg/ml of Mxra8-Fc (mouse Mxra8 fused to human IgG1 Fc region), humanized CHK-152, or humanized anti-WNV E16 (negative control) (Oliphant et al., 2005; Pal et al., 2013). Plates were washed, incubated with horseradish peroxide conjugated goat anti-human IgG (H + L) (1:5000 dilution, Jackson ImmunoResearch #109-035-088) for 1 h at 25°C, and washed again. Plates then were developed with 3,3′-5,5′ tetramethylbenzidine substrate (Thermo Fisher) and 2N H_2SO_4 and read at 450 nM using a TriStar Microplate Reader (Berthold).

Western blotting—Primary MEFs (10^6 cells, sex unknown) were harvested using TrypLE (Thermo Fisher #12605010) and lysed in 45 μL of RIPA buffer (Cell Signaling #9806S) containing protease inhibitors (Sigma Aldrich #S8830). Samples were prepared in LDS buffer (Life Technologies) under reducing (50 mM dithiothreitol) conditions. After a 70°C incubation for 10 min, samples were electrophoresed using 12% Bis-Tris gels in MOPS running buffer (Life Technologies). Proteins were transferred to PVDF membranes using an iBlot2 Dry Blotting System (Life Technologies). Membranes were blocked with 5% non-fat dry powdered milk, and probed with hamster anti-Mxra8 mAbs (3G2.F5 or 9G2.D6, 0.5 μg/ml). Western blots were incubated with Peroxidase AffiniPure goat anti-Armenian hamster IgG (H+L) (Jackson ImmunoResearch #127-035-160), and developed using SuperSignal

West Pico Chemiluminescent Substrate or SuperSignal West Femto Maximum Sensitivity Substrate (Life Technologies). To detect the truncated, soluble form of Mxra8 in the culture supernatant, MEFs were maintained in DMEM supplemented with 1% FBS in T150 flasks. One day later, supernatants were harvested and concentrated using Amicon Ultra-15 Centrifugal Filter Units (EMD Millipore #UFC900324). Concentrated supernatants were added to RIPA buffer (1X final) for western blotting analysis as described above.

Histology and RNA *in situ* hybridization—Four week-old WT and Mxra8$^{\Delta 8/\Delta 8}$ male mice were inoculated subcutaneously in the foot with 10^3 FFU of CHIKV AF15561. At 3 dpi, animals were euthanized and perfused extensively with PBS. Ipsilateral and contralateral feet were harvested and fixed in 4% paraformaldehyde (PFA) for 24 h. Tissues were decalcified in 14% EDTA free acid for two weeks and embedded in paraffin. Tissue sections were stained with hematoxylin and eosin to assess tissue morphology. To determine sites of CHIKV infection, RNA *in situ* hybridization was performed using the RNAscope 2.5 HD Assay (Brown Kit) according to the manufacturer's instructions (Advanced Cell Diagnostics). Briefly, sections were deparaffinized, treated with H_2O_2 and Protease Plus prior to probe hybridization. A probe specifically targeting the CHIKV RNA (strain AF15561) (Advanced Cell Diagnostics, #481891) was custom-designed and used for ISH experiments. Tissues were counterstained with Gill's hematoxylin. To assess the cell types that express Mxra8 RNA in naive mice, *in situ* hybridization was performed using the RNAscope 2.5 HD Assay (Red Kit). A probe specifically targeting Mxra8 (NM_024263.4) (Advanced Cell Diagnostics, #520711) was custom-designed. A negative control probe (#320751) was used in parallel. Tissue sections were visualized using a Nikon Eclipse microscope equipped with an Olympus DP71 color camera.

qRT-PCR—RNA from serum and tissues was extracted with the Viral RNA Mini Kit and RNeasy Mini Kit (QIAGEN), respectively. Viral RNA levels were determined using the TaqMan® RNA-to-Ct 1-Step Kit (Thermo Fisher #4392938) on QuantStudio 6 Flex instrument. A standard curve was produced using serial 10-fold dilutions of CHIKV RNA extracted from the viral stock. Viral burden was expressed on a $\log_{10}$ scale as viral focus-forming unit (FFU) equivalents per g of tissue or ml of serum. Primers and probes used are as follows: CHK181/AF Fwd: 5′-TCGACGCGCCATCTTTAA-3′; CHK181/AF Rev: 5′-ATCGAATGCACCGCACACT-3′; CHK181/AF Probe: 5′-/56-FAM/ACCAGCCTG/ZEN/CACCCACTCCTCAGAC/3IABkFQ/-3′; GAPDH (Mm.PT.39a.1 predesigned set, IDT); and Mxra8 (Mm.PT.58.42796673, predesigned set, IDT).

Flow cytometry—To analyze immune cells in the musculoskeletal tissues at 3 and 7 dpi, ipsilateral feet were perfused extensively, skinned, disjointed from the tibia, and digested in RPM11640 medium supplemented with 10% FBS, 15 mM HEPES, 0.5 mg/ml of collagenase (Sigma, C0130) and 10 ug/ml of DNase I (Sigma, D5025) for 1 h at 37°C. Digested tissue was passed through a 70 μm strainer, and cells were separated by centrifugation and washed with PBS supplemented with 2% FBS and 2 mM EDTA. Cells were stained with a Fixable Viability Dye eFluor 506 (eBioscience, 65-0866-14) and incubated with the following antibodies for 1 h at 4°C: CD16/32 (Biolegend, 101301, 1:200) CD11b PE-Dazzle 594 (BioLegend, 101256, 1:200), Ly6G PerCP-Cy5.5 (Biolegend,

127616, 1:400), Ly6C Pacific Blue (BioLegend, 128014, 1:200), F4/80 APC (Thermo Fisher, 17-4801-82, 1:200), CD11c PE-Cy7 (BD Biosciences, 558079, 1:200), I-A/I-E (MHC class II) Alexa Fluor 700 (BioLegend, 107622, 1:200), NK-1.1 PE (BioLegend, 108708, 1:200), CD3 BUV737 (BD Biosciences, 564380, 1:200), CD8 PerCP-Cy5.5 (BioLegend, 100734, 1:200), CD4 BV786 (BioLegend, 100552, 1:200), B220 BV711 (BioLegend, 103255, 1:200). Cells were analyzed using a BD X20 Fortessa flow cytometer, and all data were processed using FlowJo software (FlowJo, LLC).

Structural analysis of Mxra8 truncation mutants and CHIKV E2-D71 residue— The truncated forms of Mxra8 generated by the 8- or 97-bp frameshift deletions were modeled from the atomic coordinates of mouse Mxra8 (PDB 6NK3 ((Basore et al., 2019)) using PyMOL (Version 2.1.0, Schrodinger). The CHIKV E2-D71 residue was visualized on the Mxra8-bound CHIKV VLP cryo-EM model (PDB 6NK6) using PyMOL.

Cytokine and chemokine analysis—Mice were inoculated subcutaneously with 10^3 FFU of CHIKV, and the ipsilateral feet were collected at 3 and 7 dpi. Tissues were homogenized in DMEM supplemented with 2% FBS with a MagNA lyser (Roche) and analyzed for cytokine and chemokine levels using a Bio-Plex Pro Mouse Cytokine 23-plex Assay kit (Bio-Rad, #m60009rdpd) according to the manufacturer's instructions.

QUANTIFICATION AND STATISTICAL ANALYSIS

Data analysis—Statistical significance was assigned when *p values* were < 0.05 using Prism Version 8 (GraphPad). Analysis of levels of joint swelling, viral burden, cytokines and chemokines, and immune cell infiltration was determined by Mann-Whitney, one-way ANOVA, Kruskal-Wallis ANOVA, or unpaired t test depending on the data distribution and the number of comparison groups. The specific tests and numbers of experiments are indicated in the Figure legends.

DATA AND CODE AVAILABILITY

The published article includes all data generated or analyzed during this study. Original source data for Figures in the paper are available upon request to the Lead Contact author. No proprietary software was used in the data analysis.

Supplementary Material

Refer to Web version on PubMed Central for supplementary material.

ACKNOWLEDGMENTS

This study was supported by NIH grants R01AI114816, R01AI123348, and R01AI095436. We thank the Genome Engineering and iPSC Center and Department of Pathology Microinjection Facility at Washington University School of Medicine for guide RNA (gRNA) design and mouse generation, and Larissa Thackray for critical reading of the manuscript and support in the design phase of the mutant mice. We also acknowledge members of the Cherry laboratory for technical support.

REFERENCES

Ashbrook AW, Burrack KS, Silva LA, Montgomery SA, Heise MT, Morrison TE, and Dermody TS (2014). Residue 82 of the Chikungunya virus E2 attachment protein modulates viral dissemination and arthritis in mice. J. Virol 88, 12180–12192. [PubMed: 25142598]

Basore K, Kim AS, Nelson CA, Zhang R, Smith BK, Uranga C, Vang L, Cheng M, Gross ML, Smith J, et al. (2019). Cryo-EM structure of Chikungunya virus in complex with the Mxra8 receptor. Cell 177, 1725–1737.e16. [PubMed: 31080061]

Bischof J, Maeda RK, Hediger M, Karch F, and Basler K (2007). An optimized transgenesis system for Drosophila using germ-line-specific phiC31 integrases. Proc Natl Acad Sci USA 104, 3312–3317. [PubMed: 17360644]

Cancedda R, Villa-Komaroff L, Lodish HF, and Schlesinger M (1975). Initiation sites for translation of sindbis virus 42S and 26S messenger RNAs. Cell 6, 215–222. [PubMed: 1182802]

Carleton M, Lee H, Mulvey M, and Brown DT (1997). Role of glycoprotein PE2 in formation and maturation of the Sindbis virus spike. J. Virol 71, 1558–1566. [PubMed: 8995682]

Cheng RH, Kuhn RJ, Olson NH, Rossmann MG, Choi HK, Smith TJ, and Baker TS (1995). Nucleocapsid and glycoprotein organization in an enveloped virus. Cell 80, 621–630. [PubMed: 7867069]

Clark DL, Boler DD, Kutzler LW, Jones KA, McKeith FK, Killefer J, Carr TR, and Dilger AC (2011). Muscle gene expression associated with increased marbling in beef cattle. Anim. Biotechnol 22, 51–63. [PubMed: 21500107]

DeTulleo L, and Kirchhausen T (1998). The clathrin endocytic pathway in viral infection. EMBO J. 17, 4585–4593. [PubMed: 9707418]

Fox JM, Long F, Edeling MA, Lin H, van Duijl-Richter MKS, Fong RH, Kahle KM, Smit JM, Jin J, Simmons G, et al. (2015). Broadly Neutralizing Alphavirus Antibodies Bind an Epitope on E2 and Inhibit Entry and Egress. Cell 163, 1095–1107. [PubMed: 26553503]

Fox JM, Roy V, Gunn BM, Huang L, Edeling MA, Mack M, Fremont DH, Doranz BJ, Johnson S, Alter G, et al. (2019). Optimal therapeutic activity of monoclonal antibodies against chikungunya virus requires Fc-FcgammaR interaction on monocytes. Sci. Immunol 4, eaav5062. [PubMed: 30796092]

Gardner CL, Ebel GD, Ryman KD, and Klimstra WB (2011). Heparan sulfate binding by natural eastern equine encephalitis viruses promotes neurovirulence. Proc. Natl. Acad. Sci. USA 108, 16026–16031. [PubMed: 21896745]

Haist KC, Burrack KS, Davenport BJ, and Morrison TE (2017). Inflammatory monocytes mediate control of acute alphavirus infection in mice. PLoS Pathog. 13, e1006748. [PubMed: 29244871]

Han SW, Jung YK, Lee EJ, Park HR, Kim GW, Jeong JH, Han MS, and Choi JY (2013). DICAM inhibits angiogenesis via suppression of AKT and p38 MAP kinase signalling. Cardiovasc. Res 98, 73–82. [PubMed: 23386276]

Han S, Park HR, Lee EJ, Jang JA, Han MS, Kim GW, Jeong JH, Choi JY, Beier F, and Jung YK (2018). Dicam promotes proliferation and maturation of chondrocyte through Indian hedgehog signaling in primary cilia. Osteoarthritis Cartilage 26, 945–953. [PubMed: 29702220]

Han SW, Kim JM, Lho Y, Cho HJ, Jung YK, Kim JA, Lee H, Lee YJ, and Kim ES (2019). DICAM Attenuates Experimental Colitis via Stabilizing Junctional Complex in Mucosal Barrier. Inflamm. Bowel Dis 25, 853–861. [PubMed: 30534988]

Hawman DW, Stoermer KA, Montgomery SA, Pal P, Oko L, Diamond MS, and Morrison TE (2013). Chronic joint disease caused by persistent Chikungunya virus infection is controlled by the adaptive immune response. J. Virol 87, 13878–13888. [PubMed: 24131709]

Hawman DW, Fox JM, Ashbrook AW, May NA, Schroeder KMS, Torres RM, Crowe JE Jr., Dermody TS, Diamond MS, and Morrison TE (2016). Pathogenic Chikungunya Virus Evades B Cell Responses to Establish Persistence. Cell Rep 16, 1326–1338. [PubMed: 27452455]

Heidner HW, Knott TA, and Johnston RE (1996). Differential processing of sindbis virus glycoprotein PE2 in cultured vertebrate and arthropod cells. J. Virol 70, 2069–2073. [PubMed: 8627739]

Hoornweg TE, van Duijl-Richter MKS, Ayala Nuñez NV, Albulescu IC, van Hemert MJ, and Smit JM (2016). Dynamics of Chikungunya Virus Cell Entry Unraveled by Single-Virus Tracking in Living Cells. J. Virol 90, 4745–4756. [PubMed: 26912616]

Jemielity S, Wang JJ, Chan YK, Ahmed AA, Li W, Monahan S, Bu X, Farzan M, Freeman GJ, Umetsu DT, et al. (2013). TIM-family proteins promote infection of multiple enveloped viruses through virion-associated phosphatidylserine. PLoS Pathog. 9, e1003232. [PubMed: 23555248]

Jung YK, Jeong JH, Ryoo HM, Kim HN, Kim YJ, Park EK, Si HJ, Kim SY, Takigawa M, Lee BH, et al. (2004). Gene expression profile of human chondrocyte HCS-2/8 cell line by EST sequencing analysis. Gene 330, 85–92. [PubMed: 15087127]

Jung YK, Jin JS, Jeong JH, Kim HN, Park NR, and Choi JY (2008). DICAM, a novel dual immunoglobulin domain containing cell adhesion molecule interacts with alphavbeta3 integrin. J. Cell. Physiol 216, 603–614. [PubMed: 18366072]

Jung YK, Han SW, Kim GW, Jeong JH, Kim HJ, and Choi JY (2012). DICAM inhibits osteoclast differentiation through attenuation of the integrin alphaVbeta3 pathway. J. Bone Miner. Res 27, 2024–2034. [PubMed: 22492581]

Klimstra WB, Ryman KD, and Johnston RE (1998). Adaptation of Sindbis virus to BHK cells selects for use of heparan sulfate as an attachment receptor. J. Virol 72, 7357–7366. [PubMed: 9696832]

Kostyuchenko VA, Jakana J, Liu X, Haddow AD, Aung M, Weaver SC, Chiu W, and Lok SM (2011). The structure of barmah forest virus as revealed by cryo-electron microscopy at a 6-angstrom resolution has detailed transmembrane protein architecture and interactions. J. Virol 85, 9327–9333. [PubMed: 21752915]

Lee RC, Hapuarachchi HC, Chen KC, Hussain KM, Chen H, Low SL, Ng LC, Lin R, Ng MM, and Chu JJ (2013). Mosquito cellular factors and functions in mediating the infectious entry of chikungunya virus. PLoS Negl. Trop. Dis 7, e2050. [PubMed: 23409203]

Lescar J, Roussel A, Wien MW, Navaza J, Fuller SD, Wengler G, Wengler G, and Rey FA (2001). The Fusion glycoprotein shell of Semliki Forest virus: an icosahedral assembly primed for fusogenic activation at endosomal pH. Cell 105, 137–148. [PubMed: 11301009]

Levitt NH, Ramsburg HH, Hasty SE, Repik PM, Cole FE Jr., and Lupton HW (1986). Development of an attenuated strain of chikungunya virus for use in vaccine production. Vaccine 4, 157–162. [PubMed: 3020820]

Liu Y, Gordesky-Gold B, Leney-Greene M, Weinbren NL, Tudor M, and Cherry S (2018). Inflammation-Induced, STING-Dependent Autophagy Restricts Zika Virus Infection in the Drosophila Brain. Cell Host Microbe 24, 57–68.e3. [PubMed: 29934091]

Long KM, Whitmore AC, Ferris MT, Sempowski GD, McGee C, Trollinger B, Gunn B, and Heise MT (2013). Dendritic cell immunoreceptor regulates Chikungunya virus pathogenesis in mice. J. Virol 87, 5697–5706. [PubMed: 23487448]

Merkling SH, and van Rij RP (2013). Beyond RNAi: antiviral defense strategies in Drosophila and mosquito. J. Insect Physiol 59, 159–170. [PubMed: 22824741]

Morrison TE, Whitmore AC, Shabman RS, Lidbury BA, Mahalingam S, and Heise MT (2006). Characterization of Ross River virus tropism and virusinduced inflammation in a mouse model of viral arthritis and myositis. J. Virol 80, 737–749. [PubMed: 16378976]

Morrison TE, Oko L, Montgomery SA, Whitmore AC, Lotstein AR, Gunn BM, Elmore SA, and Heise MT (2011). A mouse model of chikungunya virus-induced musculoskeletal inflammatory disease: evidence of arthritis, tenosynovitis, myositis, and persistence. Am. J. Pathol 178, 32–40. [PubMed: 21224040]

Mulvey M, and Brown DT (1995). Involvement of the molecular chaperone BiP in maturation of Sindbis virus envelope glycoproteins. J. Virol 69, 1621–1627. [PubMed: 7853497]

Oliphant T, Engle M, Nybakken GE, Doane C, Johnson S, Huang L, Gorlatov S, Mehlhop E, Marri A, Chung KM, et al. (2005). Development of a humanized monoclonal antibody with therapeutic potential against West Nile virus. Nat. Med 11, 522–530. [PubMed: 15852016]

Pal P, Dowd KA, Brien JD, Edeling MA, Gorlatov S, Johnson S, Lee I, Akahata W, Nabel GJ, Richter MKS, et al. (2013). Development of a highly protective combination monoclonal antibody therapy against Chikungunya virus. PLoS Pathog. 9, e1003312. [PubMed: 23637602]

Paredes AM, Brown DT, Rothnagel R, Chiu W, Schoepp RJ, Johnston RE, and Prasad BV (1993). Three-dimensional structure of a membrane-containing virus. Proc. Natl. Acad. Sci. USA 90, 9095–9099. [PubMed: 8415660]

Poo YS, Nakaya H, Gardner J, Larcher T, Schroder WA, Le TT, Major LD, and Suhrbier A (2014). CCR2 deficiency promotes exacerbated chronic erosive neutrophil-dominated chikungunya virus arthritis. J. Virol 88, 6862–6872. [PubMed: 24696480]

Powers AM, Brault AC, Shirako Y, Strauss EG, Kang W, Strauss JH, and Weaver SC (2001). Evolutionary relationships and systematics of the alphaviruses. J. Virol 75, 10118–10131. [PubMed: 11581380]

Rose PP, Hanna SL, Spiridigliozzi A, Wannissorn N, Beiting DP, Ross SR, Hardy RW, Bambina SA, Heise MT, and Cherry S (2011). Natural resistance-associated macrophage protein is a cellular receptor for sindbis virus in both insect and mammalian hosts. Cell Host Microbe 10, 97–104. [PubMed: 21843867]

Seymour RL, Rossi SL, Bergren NA, Plante KS, and Weaver SC (2013). The role of innate versus adaptive immune responses in a mouse model of O'nyong-nyong virus infection. Am. J. Trop. Med. Hyg 88, 1170–1179. [PubMed: 23568285]

Silva LA, Khomandiak S, Ashbrook AW, Weller R, Heise MT, Morrison TE, and Dermody TS (2014). A single-amino-acid polymorphism in Chikungunya virus E2 glycoprotein influences glycosaminoglycan utilization. J. Virol 88, 2385–2397. [PubMed: 24371059]

Smith TJ, Cheng RH, Olson NH, Peterson P, Chase E, Kuhn RJ, and Baker TS (1995). Putative receptor binding sites on alphaviruses as visualized by cryoelectron microscopy. Proc. Natl. Acad. Sci. USA 92, 10648–10652. [PubMed: 7479858]

Song H, Zhao Z, Chai Y, Jin X, Li C, Yuan F, Liu S, Gao Z, Wang H, Song J, et al. (2019). Molecular Basis of Arthritogenic Alphavirus Receptor MXRA8 Binding to Chikungunya Virus Envelope Protein. Cell 177, 1714–1724.e12. [PubMed: 31080063]

Sourisseau M, Schilte C, Casartelli N, Trouillet C, Guivel-Benhassine F, Rudnicka D, Sol-Foulon N, Le Roux K, Prevost MC, Fsihi H, et al. (2007). Characterization of reemerging chikungunya virus. PLoS Pathog. 3, e89. [PubMed: 17604450]

Strauss JH, Wang KS, Schmaljohn AL, Kuhn RJ, and Strauss EG (1994). Host-cell receptors for Sindbis virus. Arch. Virol. Suppl 9, 473–484. [PubMed: 7913360]

Teo TH, Lum FM, Claser C, Lulla V, Lulla A, Merits A, Rénia L, and Ng LF (2013). A pathogenic role for CD4+ T cells during Chikungunya virus infection in mice. J. Immunol 190, 259–269. [PubMed: 23209328]

Tsetsarkin K, Higgs S, McGee CE, De Lamballerie X, Charrel RN, and Vanlandingham DL (2006). Infectious clones of Chikungunya virus (La Réunion isolate) for vector competence studies. Vector Borne Zoonotic Dis 6, 325–337. [PubMed: 17187566]

Voss JE, Vaney MC, Duquerroy S, Vonrhein C, Girard-Blanc C, Crublet E, Thompson A, Bricogne G, and Rey FA (2010). Glycoprotein organization of Chikungunya virus particles revealed by X-ray crystallography. Nature 468, 709–712. [PubMed: 21124458]

Wang KS, Kuhn RJ, Strauss EG, Ou S, and Strauss JH (1992). High-affinity laminin receptor is a receptor for Sindbis virus in mammalian cells. J. Virol 66, 4992–5001. [PubMed: 1385835]

Wang T, Birsoy K, Hughes NW, Krupczak KM, Post Y, Wei JJ, Lander ES, and Sabatini DM (2015). Identification and characterization of essential genes in the human genome. Science 350, 1096–1101. [PubMed: 26472758]

Wintachai P, Wikan N, Kuadkitkan A, Jaimipuk T, Ubol S, Pulmanausahakul R, Auewarakul P, Kasinrerk W, Weng WY, Panyasrivanit M, et al. (2012). Identification of prohibitin as a Chikungunya virus receptor protein. J. Med. Virol 84, 1757–1770. [PubMed: 22997079]

Yonezawa T, Ohtsuka A, Yoshitaka T, Hirano S, Nomoto H, Yamamoto K, and Ninomiya Y (2003). Limitrin, a novel immunoglobulin superfamily protein localized to glia limitans formed by astrocyte endfeet. Glia 44, 190–204. [PubMed: 14603461]

Zhang W, Heil M, Kuhn RJ, and Baker TS (2005). Heparin binding sites on Ross River virus revealed by electron cryo-microscopy. Virology 332, 511–518. [PubMed: 15680416]

Zhang R, Kim AS, Fox JM, Nair S, Basore K, Klimstra WB, Rimkunas R, Fong RH, Lin H, Poddar S, et al. (2018). Mxra8 is a receptor for multiple arthritogenic alphaviruses. Nature 557, 570–574. [PubMed: 29769725]

Highlights

- Reduced infection of four different alphaviruses is seen in Mxra8-deficient mice
- Reduced CHIKV-induced joint swelling is observed in Mxra8-deficient mice
- D71A mutant CHIKV that lacks binding to Mxra8 is attenuated in wild-type mice
- Ectopic Mxra8 expression is sufficient to enhance CHIKV infection in *Drosophila*

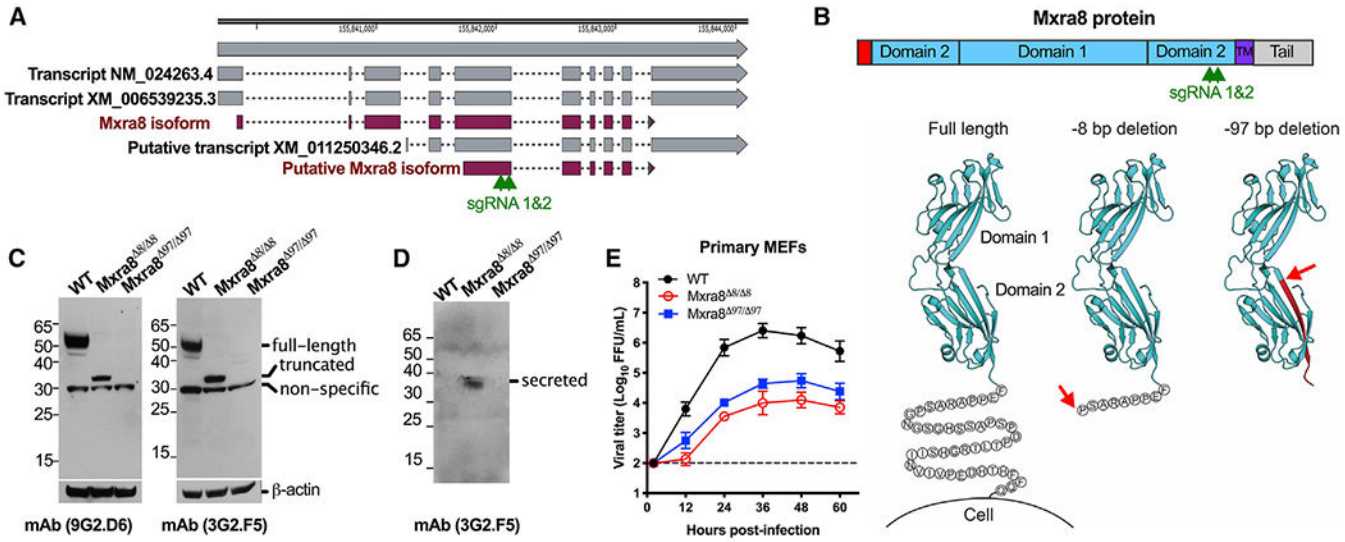

Figure 1. Generation of *Mxra8*-Deficient Mice by CRISPR-Cas9 Gene Targeting

(A) Scheme of *Mxra8* gene locus with sgRNA targeting sites. Annotated transcripts are shown in gray and encoded proteins in purple. Two green arrows indicate the sgRNA targeting sites.

(B) Location of Mxra8 proteins (8- and 97-nt frameshift deletions) on the X-ray crystal structure of mouse Mxra8 (PDB: 6NK3). The structurally unsolved regions adjacent to the plasma membrane are shown as circled amino acids, and the ends of Mxra8 proteins generated by the gene-editing deletions are indicated by arrows. TM, transmembrane; tail, cytoplasmic domain.

(C and D) Western blotting of cell lysates (C) or culture supernatants (D) of primary MEFs from WT, $Mxra8^{\Delta 8/\Delta 8}$, and $Mxra8^{\Delta 97/\Delta 97}$ mice using two different anti-Mxra8 mAbs. Data are representative of two experiments.

(E) Growth kinetic analysis of CHIKV-AF15561 (MOI 0.01) in primary MEFs from WT, $Mxra8^{\Delta 8/\Delta 8}$, and $Mxra8^{\Delta 97/\Delta 97}$ mice. Data are pooled from two experiments (n = 6).

See also Figures S1 and S2.

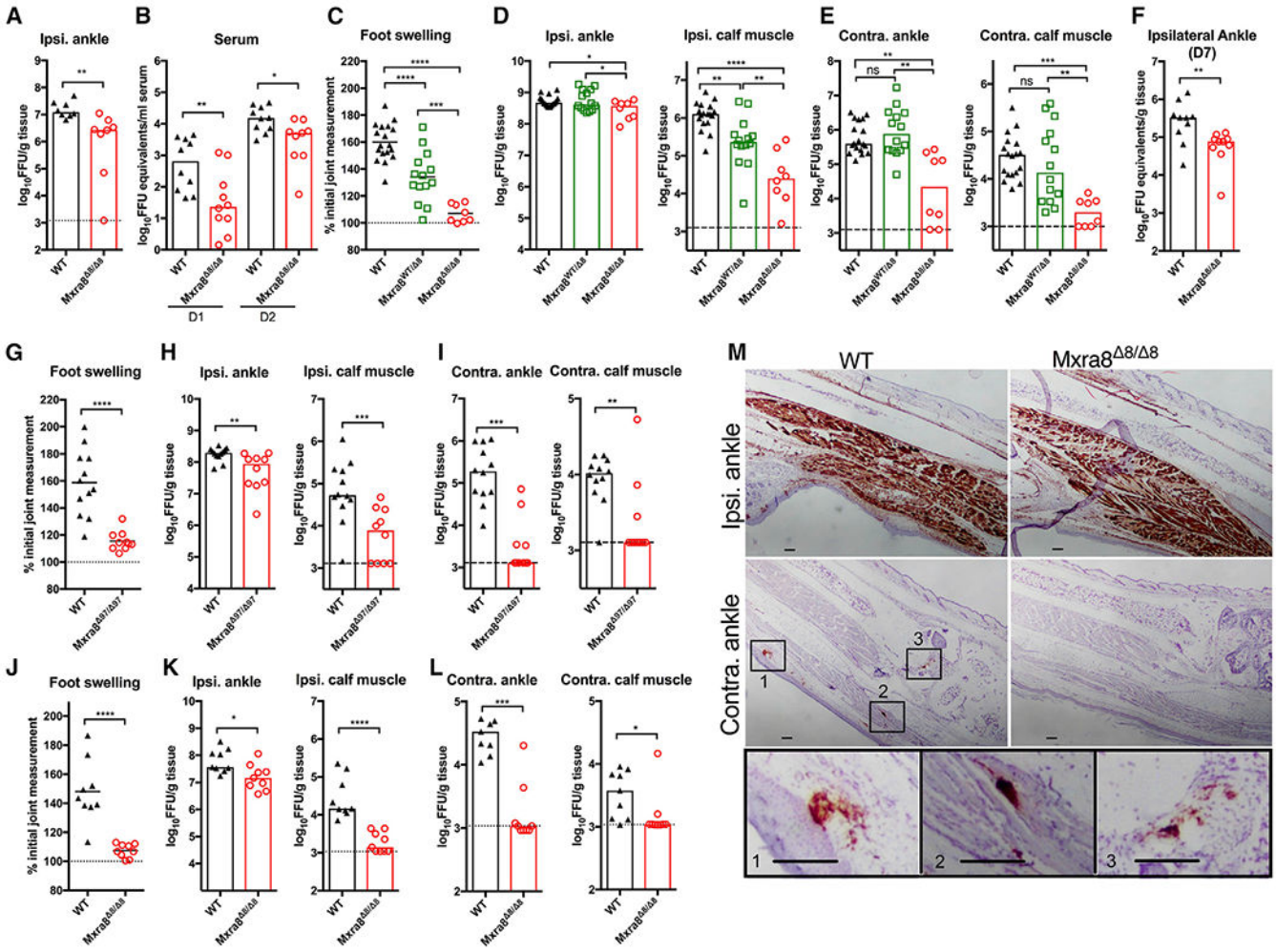

Figure 2. CHIKV Infection in *Mxra8*-Deficient Mice during the Acute Phase after Subcutaneous Inoculation

(A and B) WT and *Mxra8*$^{\Delta 8/\Delta 8}$ mice were inoculated subcutaneously in the foot with 10^3 focus-forming units (FFU) of CHIKV-AF15561. (A) At 12 h post-infection, the ipsilateral ankle were harvested for virus titration by FFU assay (two experiments; n = 8; two-tailed Mann-Whitney test; **p < 0.01; ns, not significant). (B) At 1 and 2 dpi, serum was collected for viral RNA quantification by qRT-PCR (two experiments; n = 9–10; two-tailed Mann-Whitney test; *p < 0.05 and **p < 0.01).

(C–F) WT, *Mxra8*$^{+/\Delta 8}$, or *Mxra8*$^{\Delta 8/\Delta 8}$ mice were inoculated subcutaneously in the foot with 10^3 FFU of CHIKV-AF15561. At 3 (C–E) or 7 dpi (F), foot swelling (C) was measured (two experiments; n = 8–18; one-way ANOVA with Tukey's test; ***p < 0.001 and ****p < 0.0001), and ipsilateral and contralateral ankles and calf muscles (D–F) were harvested for virus titration by FFU assay (two experiments; n = 8–18; (D), one-way ANOVA with Tukey's test; (E) Kruskal-Wallis with Dunn's test; (F) two-tailed Mann-Whitney test; *p < 0.05, **p < 0.01, ***p < 0.001, and ****p < 0.0001; ns, not significant).

(G–L) WT and *Mxra8*$^{\Delta 97/\Delta 97}$ (G–I) or WT and *Mxra8*$^{\Delta 8/\Delta 8}$ (J–L) mice were inoculated subcutaneously in the foot with 10^3 FFU of CHIKV-AF15561 (G–I) or CHIKV-LR 2006 (J–L). At 3 dpi, foot swelling (G and J) was measured (two experiments; n = 9–12; two-tailed

unpaired t test; ****$p < 0.0001$), and ipsilateral and contralateral ankles and calf muscles (H, I, K, and L) were harvested for virus titration by FFU assay (two experiments; n = 9–12; two-tailed Mann-Whitney test; *$p < 0.05$, **$p < 0.01$, ***$p < 0.001$, and ****$p < 0.0001$). (M) RNA *in situ* hybridization of ipsilateral and contralateral feet using a CHIKV-specific probe from WT and *Mxra8*$^{\Delta 8/\Delta 8}$ mice at 3 dpi. CHIKV RNA^{+} foci in the contralateral ankles of WT mice are boxed and shown below as higher-magnification images. Scale bar, 100 βm; representative images are shown from n = 4 mice from two experiments.
See also Figure S3.

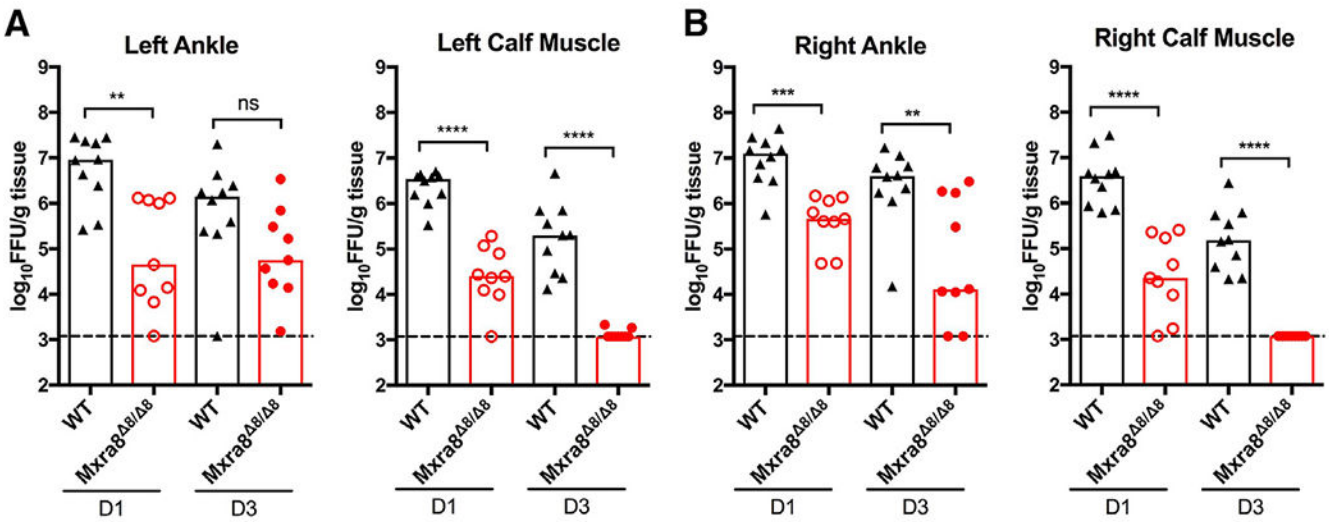

Figure 3. CHIKV Infection in *Mxra8*-Deficient Mice during the Acute Phase after Intravenous Inoculation

WT and *Mxra8*$^{\Delta 8/\Delta 8}$ mice were inoculated intravenously via the tail vein with 10^3 FFU of CHIKV-AF15561. At 1 and 3 dpi, ankle and calf muscle from both left (A) and right (B) sides were collected for virus titration by FFU assay (two experiments, n = 9–10; two-tailed Mann-Whitney test;**p <0.01, ***p < 0.001, and ****p < 0.0001; ns, not significant).

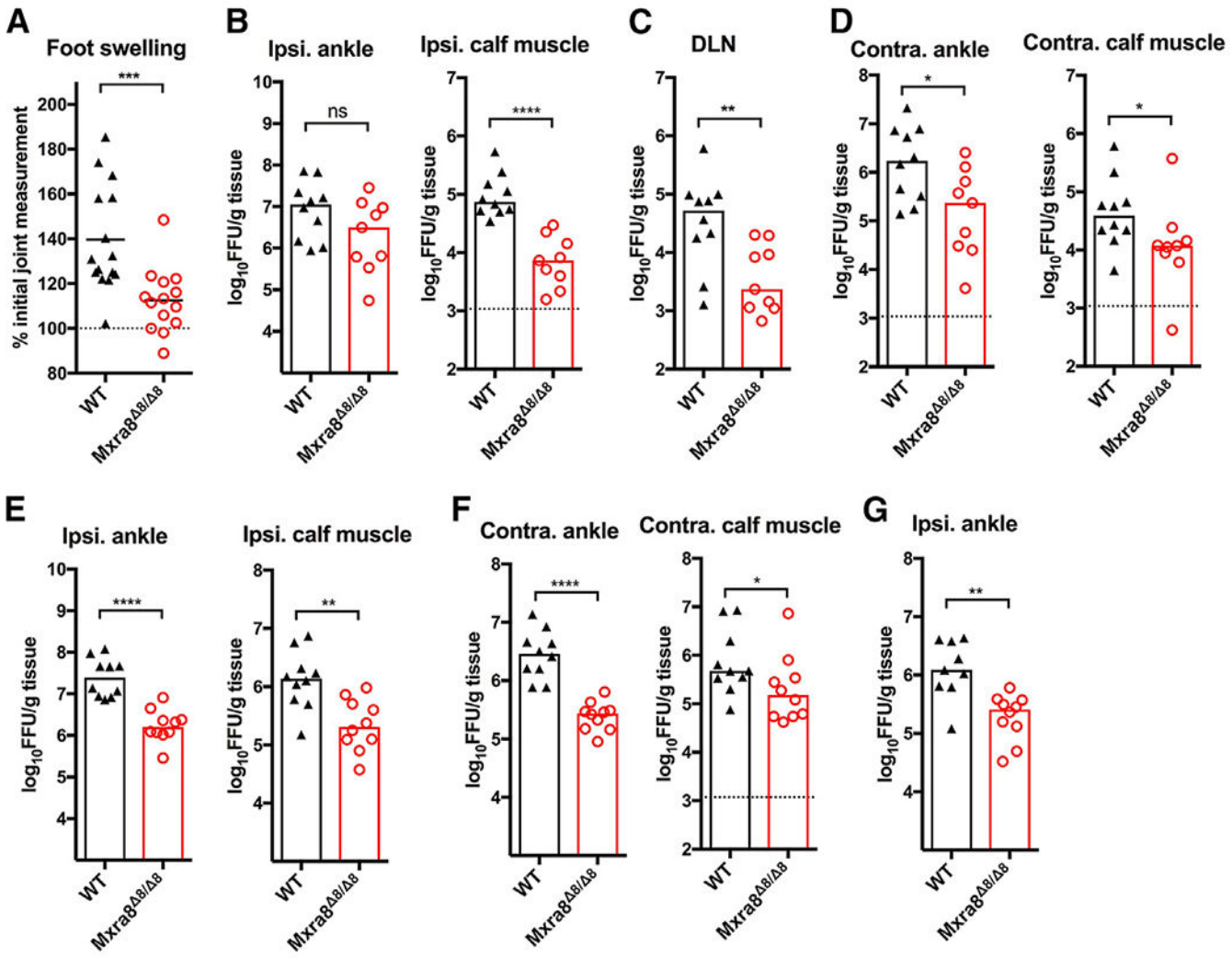

Figure 4. Diminished Infection of MAYV, RRV, and ONNV in *Mxra8*$^{\Delta 8/\Delta 8}$ Mice

WT and *Mxra8*$^{\Delta 8/\Delta 8}$ mice were inoculated subcutaneously in the foot with 10^3 FFU of MAYV (A–D), 10^3 FFU of RRV (E and F), or 10^3 FFU of ONNV (G). Foot swelling of MAYV infection (A) at 3 dpi was measured (two experiments; n = 14–15; two--tailed unpaired t test; ***p < 0.001). Ipsilateral and contralateral ankles and calf muscles at 12 h (G) and 3 dpi (B–F) were harvested for virus titration by FFU assay (two experiments; n = 9–15; two-tailed Mann-Whitney test; *p < 0.05, **p < 0.01, ***p < 0.001, and ****p < 0.0001; ns, not significant).

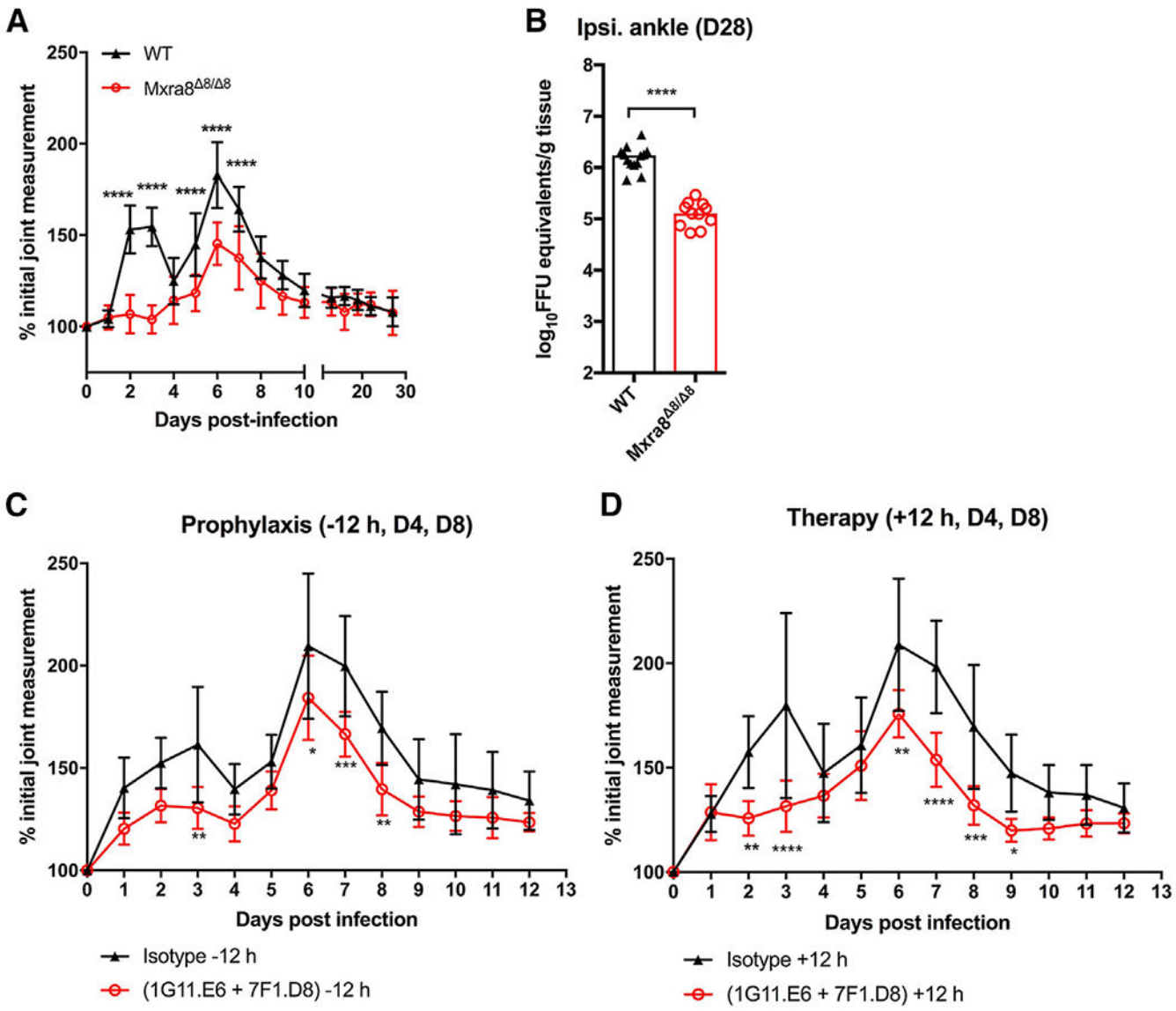

Figure 5. CHIKV Infection and Disease in *Mxra8*$^{\Delta 8/\Delta 8}$ Mice or WT Mice Treated with Blocking Anti-Mxra8 mAbs

(A and B) WT and *Mxra8*$^{\Delta 8/\Delta 8}$ mice were inoculated subcutaneously in the foot with 10^3 FFU of CHIKV-AF15561. (A) Foot swelling was measured daily for 28 days (two experiments; n = 11–13; means ± SEMs; two-way ANOVA with Sidak's test; ****p < 0.0001). (B) Ipsilateral ankles were collected at 28 dpi, and viral RNA levels were measured by qRT-PCR (two experiments; n = 11–13; two-tailed Mann-Whitney test; ****p< 0.0001). (C and D) WT mice were inoculated subcutaneously in the foot with 10^3 FFU of CHIKV-AF15561 and then administered either anti-Mxra8 mAbs (1G11.E6 + 7F1.D8; 300 μg total) or isotype control hamster mAb (300 μg) via an intraperitoneal injection at −12 h (C) or +12 h (D) post-infection. Subsequent doses of mAbs were administered at 4 and 8 dpi. Foot swelling was measured daily for 12 days (two experiments; n = 8; means ± SEMs; two-way ANOVA with Sidak's test; *p < 0.05, **p < 0.01, ***p < 0.001, and ****p < 0.0001).

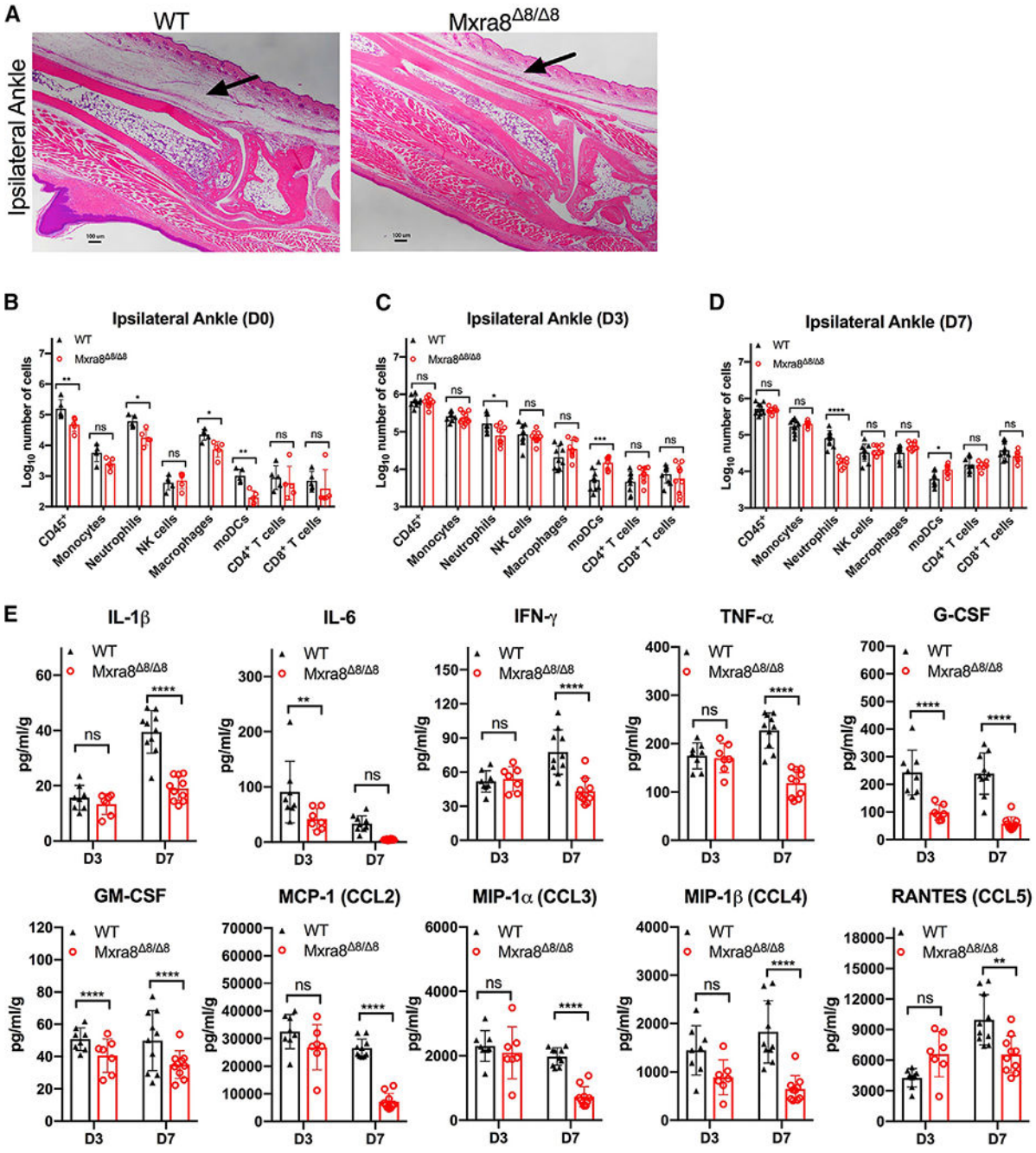

Figure 6. Analysis of Inflammation in the Musculoskeletal Tissues of *Mxra8*$^{\Delta 8/\Delta 8}$ Mice after CHIKV Infection

(A–D) WT and *Mxra8*$^{\Delta 8/\Delta 8}$ mice were inoculated subcutaneously in the foot with 10^3 FFU of CHIKV-AF15561.

(A) At 3 dpi, ipsilateral feet were collected, fixed, decalcified, paraffin embedded, sectioned, and stained with H&E. Scale bar, 100 μm; representative images are shown from n = 4 mice from two experiments. Arrows indicate tissue edema. At days 0 (B) (uninfected), 3 (C), and 7 (D) post-infection, cells from ipsilateral feet were harvested and analyzed for numbers of leukocytes ($CD45^+$), monocytes ($CD11b^+CD11c^-Ly6G^-Ly6C^+$), neutrophils (CD11b

$^{+}$CD11c^{-}Ly6G^{+}), natural killer(NK) cells (CD3^{-}NK1.1^{+}), macrophages (CD11b^{+}CD11c^{-}Ly6G^{-}Ly6C^{-}F4/80^{+}), monocyte-derived dendritic cells (DCs) (CD11b^{+}CD11c^{+}Ly6G^{-}Ly6C^{+}MHCII^{+}), CD4^{+} T cells (CD3^{+}CD4^{+}), and CD8^{+} T cells (CD3^{+}CD8^{+}) by flow cytometry (see Figure S4 for gating scheme, two experiments; n = 8–10; two-tailed Mann-Whitney test; *p < 0.05, **p < 0.01, ***p < 0.001, and ****p < 0.0001; ns, not significant). (E) At 3 and 7 dpi, ipsilateral ankles from WT and *Mxra8*$^{\Delta 8/\Delta 8}$ mice were harvested, homogenized, and the indicated cytokines or chemokines were measured (two experiments; n = 8–10, mean ± SD; two-way ANOVA with Sidak's test; *p < 0.05; **p < 0.01; ****p < 0.0001; ns, not significant).

See also Figures S4 and S5.

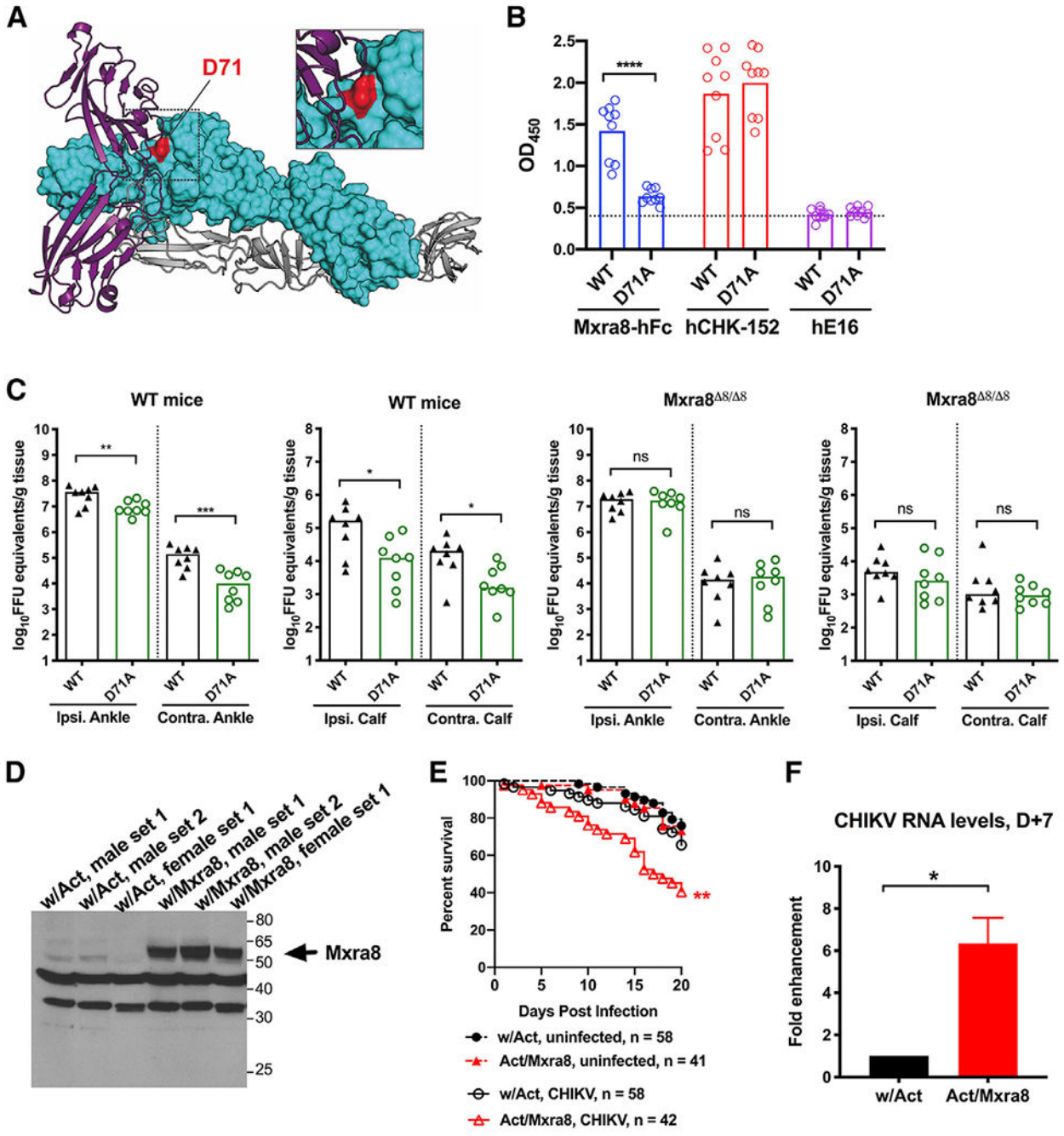

Figure 7. Loss- and Gain-of-Function Effects of Mxra8 in Mice and *Drosophila*

(A) Structural representation of the CHIKV E2-D71 residue (red) on the cryoelectron microscopy (cryo-EM) model of Mxra8 bound to CHIKV (PDB 6NK6). Color scheme: Mxra8, purple; CHIKV E2, cyan; and CHIKV E1, gray. Inset: magnified view of the Mxra8-CHIKV E2-D71 interface.

(B) Loss of binding to Mxra8 by D71A mutation in CHIKV. WT and D71A CHIKV were captured with mouse CHK-152 (anti-E2) and CHK-166 mAb (anti-E1). After washing, Mxra8-Fc(human IgG1 Fc)was added and binding was measured. Equivalent amounts of

WT and D71A CHIKV were captured on the microtiter plate as determined by the binding of humanized CHK-152. Humanized E16 (anti-West Nile virus [WNV] E) served as a negative control. Results are the mean of three experiments performed in triplicate (Mann-Whitney test: ****$p < 0.0001$).

(C) WT and *Mxra8*$^{\Delta 8/\Delta 8}$ mice were inoculated subcutaneously in the foot with 10^3 FFU of CHIKV-AF15561 (WT or D71A mutant). At 3 dpi, tissues were harvested for virus titration by FFU assay(two experiments; n = 8; two-tailed Mann-Whitney test; *$p < 0.05$, **$p < 0.01$, and ***$p < 0.001$; ns, not significant).

(D–F) Transgenic flies expressing mouse Mxra8 have increased susceptibility to CHIKV infection.(D) Flies of the indicated genotypes were analyzed for the ectopic expression of Mxra8 by western blotting. (E) The indicated flies were either uninfected or challenged with CHIKV (strain 181/25) and monitored daily for mortality. Data are pooled from three experiments and the number of flies are indicated (log rank test; **$p < 0.01$). (F) Groups of 15 flies of the indicated genotype were inoculated with CHIKV, and total RNA was collected at 7 dpi. Viral RNA was quantified by qRT-PCR, normalized to the housekeeping gene rp49, and shown relative to control (Act > +). Means ± SEMs are shown for four experiments (unpaired t test; *$p < 0.05$).

KEY RESOURCES TABLE

REAGENT or RESOURCE	SOURCE	IDENTIFIER
Antibodies		
Anti-Mxra8 1G11.E6	Zhang et al., 2018; PMID 29769725	N/A
Anti-Mxra8 3G2.F5	Zhang et al., 2018; PMID 29769725	N/A
Anti-Mxra8 7F1.D8	Zhang et a., 2018; PMID 29769725	N/A
Anti-Mxra8 9G2.D6	Zhang et al., 2018; PMID 29769725	N/A
Armenian Hamster IgG Isotype Control	Bio X Cell	BE0260
CHK-152	Pal et al., 2013; PMID 24829346	N/A
CHK-166	Pal et al., 2013; PMID 24829346	N/A
Humanized CHK-152	Pal et al., 2013; PMID 24829346	N/A
Humanized CHK-166	Pal et al., 2013; PMID 24829346	N/A
Humanized E16	Oliphant et al., 2005; PMID 15852016	N/A
Peroxidase AffiniPure Goat Anti-Human IgG (H+L)	Jackson ImmunoResearch	109-035-088
Peroxidase AffiniPure Goat Anti-Armenian Hamster IgG (H+L)	Jackson ImmunoResearch	127-035-160
Alexa Fluor 647 Goat Anti-Armenian Hamster IgG H&L	Abcam	ab173004
Anti-Mouse CD16/32 Antibody	BioLegend	101301
PE/Dazzle 594 Anti-Mouse/Human CD11b Antibody	BioLegend	101256
PerCP/Cy5.5 Anti-Mouse Ly-6G Antibody	BioLegend	127616
Pacific Blue Anti-Mouse Ly-6C Antibody	BioLegend	128014
APC F4/80 Monoclonal Antibody (BM8)	Thermo Fisher	17-4801-82
PE-Cy7 Hamster Anti-Mouse CD11c Antibody	BD Biosciences	558079
Alexa Fluor 700 Anti-Mouse I-A/I-E Antibody	BioLegend	107622
PE Anti-Mouse NK-1.1 Antibody	BioLegend	108708
BUV737 Rat Anti-Mouse CD3 Antibody	BD Biosciences	564380
PerCP/Cyanine5.5 Anti-Mouse CD8a Antibody	BioLegend	100734
Brilliant Violet 785 Anti-Mouse CD4 Antibody	BioLegend	100552
Brilliant Violet 711 Anti-Mouse/Human CD45R/B220 Antibody	BioLegend	103255
Bacterial and Virus Strains		
Chikungunya virus (strain LR 2006)	Tsetsarkin et al., 2006; PMID 17187566	GenBank Accession No: KY575571
Chikungunya virus (strain AF15561)	Hawman et al., 2016; PMID 27452455	GenBank Accession No: EF452493
Chikungunya virus E2-D71A mutant (strain AF15561)	This study	N/A
Chikungunya virus (strain 181/25)	Levitt et al., 1986; PMID 3020820	GenBank Accession No: AF192908
Ross River virus (strain T48)	World Reference Center for Emerging Viruses and Arboviruses	GenBank Accession number ACV67002
Mayaro virus (strain BeH407)	World Reference Center for Emerging Viruses and Arboviruses	GenBank Accession number AAY45742
O'nyong nyong virus (strain MP30)	World Reference Center for Emerging Viruses and Arboviruses	GenBank Accession number AAC97207

REAGENT or RESOURCE	SOURCE	IDENTIFIER
Chemicals, Peptides, and Recombinant Proteins		
Mammalian-expressed, codon-optimized mouse Mxra8 fused to human IgG1 Fc region	This study	N/A
Fixable Viability Dye eFluor 506	eBioscience	65-0866-14
Collagenase	Sigma-Aldrich	C0130
Deoxyribonuclease I	Sigma-Aldrich	D5025
Critical Commercial Assays		
MEGAscript T7 Transcription Kit	Thermo Fisher	AM1334
MEGAclear Transcription Clean-Up Kit	Thermo Fisher	AM1908
mMESSAGE mMACHINE SP6 Transcription Kit	Thermo Fisher	AM1340
In-Fusion HD Cloning Plus	Takara	638910
RNAscope 2.5 HD Assay (Brown Kit)	Advanced Cell Diagnostics	322310
RNAscope 2.5 HD Assay (Red Kit)	Advanced Cell Diagnostics	322360
TaqMan RNA-to-Ct 1-Step Kit	Thermo Fisher	4392938
Bio-Plex Pro Mouse Cytokine 23-plex Assay Kit	Bio-Rad	m60009rdpd
Deposited Data		
X-ray crystal structure of murine Mxra8	Basore et al., 2019	PDB 6NK3
Electron Cryo-Microscopy of Chikungunya VLP in complex with mouse Mxra8 receptor	Basore et al., 2019	PDB 6NK6; EMD-9394
Experimental Models: Cell Lines		
BHK-21	ATCC	CCL-10
Vero	ATCC	CCL-81
C57BL/6J primary MEF	This study	N/A
C57BL/6J Mxra8$^{\Delta 8/\Delta 8}$ primary MEF	This study	N/A
C57BL/6J Mxra8$^{\Delta 97/\Delta 97}$ primary MEF	This study	N/A
Experimental Models: Organisms/Strains		
Mouse: C57BL/6J	The Jackson Laboratory	000664
Mouse: C57BL/6J Mxra8$^{+/\Delta 8}$	This study	N/A
Mouse: C57BL/6J Mxra8$^{\Delta 8/\Delta 8}$	This study	N/A
Mouse: C57BL/6J Mxra8$^{\Delta 97/\Delta 97}$	This study	N/A
D. melanogaster: Actin-Gal4	Bloomington Drosophila Stock Center	BDSC:4414; FlyBase: FBst0004414
D. melanogaster: Actin-Mxra8	Rainbow Transgenic Flies; This study	N/A
Oligonucleotides		
Mxra8_sgRNA-1: 5′-GGAAGACTCGGCGCT CGTGG-3′	Genome Engineering and iPSC Center, Washington University in St. Louis	N/A
Mxra8_sgRNA-2: 5′-CTGTGACCAGACCCA TTGCC-3′	Genome Engineering and iPSC Center, Washington University in St. Louis	N/A
CHIKV FOR: GGCAGTGGTCCCAGATAATTCAAG	This study	N/A
CHIKV FOR: ACTGTCTAGATCCACCCCATACATG	This study	

REAGENT or RESOURCE	SOURCE	IDENTIFIER
Drosophila rp49 FOR: AAGAAGCGCACCAAACACTTCATC	Liu et al., 2018 PMID:29934091	N/A
Drosophila rp49 REV: TCTGTTGTCGATACCCTTCGGCTT	Liu et al., 2018 PMID:29934091	N/A
CHK181/AF Fwd: 5′-TCGACGCGCCATCTTTAA-3′	IDT	N/A
CHK181/AF Rev: 5′-ATCGAATGCACCGCACACT-3′	IDT	N/A
CHK181/AF Probe: 5′-/56-FAM/ACCAGCCTG/ZEN/ CACCCACTCCTCAGAC/3IABkFQ/-3′	IDT	N/A
GAPDH TaqMan Primer/Probe set	IDT	Mm.PT.39a.1
Mxra8 TaqMan Primer/Probe set	IDT	Mm.PT.58.42796673
CHIKV RNA ISH probe	Advanced Cell Diagnostics	481891
Mxra8 RNA ISH probe	Advanced Cell Diagnostics	520711
Control RNA ISH probe	Advanced Cell Diagnostics	320751
Recombinant DNA		
pUASTattB vector	Bischof et al., 2007 PMID:17360644	N/A
Codon-optimized mouse Mxra8 cloned into pUASTattB vector	This study	N/A
CHIKV AF15561 plasmid	Ashbrook et al., 2014; PMID 25142598	
CHIKV AF15561 E2-D71A plasmid	This study	N/A
Codon-optimized mouse Mxra8 and human IgG1 Fc cloned into pCDNA3.4 vector	This study	N/A
Software and Algorithms		
FlowJo	FlowJo, LLC	Version 10
PyMOL	Schrodinger	Version 2.1.0
GraphPad Prism	GraphPad	Version 8.1.1